

Department of Environment Systems
Graduate School of Frontier Sciences
The University of Tokyo

2019
Master's Thesis

**The Importance of Phase Transition in Closed
Loop Geothermal Power Generation System
Using CO₂ as Working Fluid**

(CO₂を駆動流体とする Closed Loop 地熱発電
システムにおける相変化の重要性)

Submitted January 23, 2020
Supervisor: Assist. Prof. Masaatsu AICHI

馬 振宇

Ma Zhenyu

Content

Chapter 1 : General Introduction	1
1.1 Background	1
1.2 Geothermal Power Generation	3
1.3 Existent Difficulties in Popularizing Geothermal	5
1.3.1 Initial Cost.....	5
1.3.2 Environment concerns.....	6
1.3.3 Induced Seismic Activity	8
1.3.4 Relative Technology Development	10
1.4 Enhanced Geothermal System (EGS)	12
1.4.1 What is EGS ?	12
1.4.2 Advantages of Using CO ₂ as Working Fluid	14
1.4.3 Current state of EGS development	16
Chapter 2 : Methodology	17
2.1 Introduction	17
2.2 Mathematical Formulation	19
2.2.1 Mass and Energy Conservation Equations.....	19
2.2.2 Momentum Conservation (Drift-Flux Model).....	21
2.2.3 Discretized Equations	27
2.3 Space and Time Discretization	31
2.4 Closed-Loop Heat Exchange Method	35
2.4.1 Various Configurations of Closed Loop System (CLS)	35
2.4.2 ECO ₂ G	37
2.4.3 ECO ₂ G versus Conventional Geothermal	40
2.4.4 Example problems as demonstration for reliability of T2Well	42
Chapter 3 : Model Information	52
3.1 Introduction for Construction of model	52
3.2 Preparation of Input Data	56
3.2.1 Initial Condition	56
3.2.2 Boundary Condition	60

Chapter 4 : Results and Analysis	61
4.1 Temperature	61
4.2 Density and Phase Transition	63
4.3 Energy gain	69
4.4 Sustainability	71
4.5 Cost and Profit	74
4.5.1 Heat Exchanger Costs.....	74
4.5.2 Turbine Costs.....	78
4.5.3 Well Costs.....	80
4.5.4 Total Capital cost.....	82
Chapter 5 : Conclusion	84
References	85
Acknowledgement	89

Chapter 1: General Introduction

1.1 Background

Inside the earth, the thermal energy that exists in the shallow part, usually within a few kilometers from surface of Earth, and can be used by humans is called geothermal energy. There is a tremendous amount of thermal energy in the shallow part of the Earth that cannot be used up. It is estimated to be about 6000°C at the depth of 6370km, the center of Earth, which is almost the same level as the surface temperature of the sun. Also, 99% of the earth's volume is above 1000°C , and the portion below 100°C is only 0.1%. Since the Earth's interior is hot and the Earth's surface is at a low temperature of about 15°C , heat naturally flows out of the Earth. However, even heat flows from interior of Earth at natural rate, it will take billions of years for the Earth to cool. Therefore, it is considered that heat energy stored inside the Earth is inexhaustible.

The current technology cannot use the high-temperature heat as described above. The rain that has fallen penetrates underground (several kilometers deep), is warmed by hot rocks, heated water is called hot water, and is occurred in relatively shallow area. It is used by removing steam and hot water from a place (geothermal reservoir) reserved in a section (1~3 km deep) by boring. The hot water effuses to the surface naturally is called hot spring. Near the volcano, it is hotter than general places in the shallower area. That is because high-temperature magma exists in the deep part of the volcano. Therefore, some geothermal reservoirs are created in the shallower part of the magma. Figure 1 shows the production and reduction wells excavated in the geothermal reservoir (natural boiler) heated by the magma chamber and the geothermal power generation equipment on the ground.

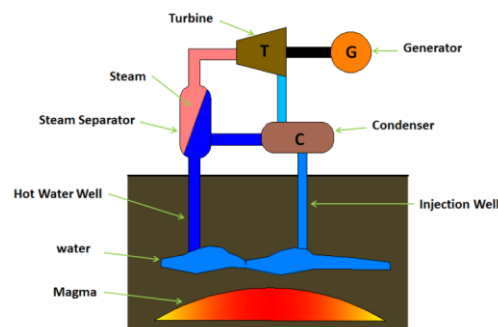


Figure 1. Magma power generation using high heat near the magma chamber

Based on a numerical model of underground heat and water flow, it is possible to examine how much power generation geothermal can produce. A numerical model can be used to calculate how much steam can be produced at specified depth by drilling. You can also simulate how the underground changes when steam is produced. Thus, if you know the amount of steam produced, you can calculate how much power can be generated. As a result, depending on how many production wells are drilled and how many reduction wells are drilled, it is possible to determine how much power generation scales will produce power stably over the long term.

Currently, it is calculated by setting what kind of power generation method to select or how many years to extract heat. In many cases, the scale of power generation is determined by extracting heat in about 30 years. However, since the heat is not actually lost and it is replenished naturally, power generation occurs semi-permanently.

With the continuous growth of the world economy, the consumption of energy is also increasing, and the large-scale use of fossil fuels not only brings serious environmental pollution and ecological damage, but also decreases the amount of resources. Therefore, the usage of clean renewable energy meets the urgent needs of sustainable development. As one of the alternative energy sources, geothermal energy is receiving increasing attention. Geothermal power stations have no fuel transportation equipment, no huge boiler equipment, and no environmental pollution caused by slag and flue gas, which is relatively clean. Plus, the cost of electricity generation is lower than hydropower and thermal power.

Coal and oil have been the mainstream energy of the earth for hundreds of years. According to estimates of global reserves and consumption speed, It is afraid that oil and coal can only serve humanity for another 200 years. Therefore, the transformation of energy is imperative. Among many varieties of new energy, the development of geothermal technology with huge underground reserves will become one of the key technologies to change the world in the process of energy upgrade.

1.2 Geothermal Power Generation

Geothermal power generation is a new power generation technology that uses underground hot water and steam as power sources. Its basic principle is similar to that of thermal power generation. It is also based on the principle of energy conversion. First of all, geothermal energy is converted into mechanical energy, and then mechanical energy is converted into electrical energy. Geothermal power generation is actually an energy conversion process that converts thermal power underground into mechanical energy, and then converts mechanical energy into electrical energy on the surface.

Compared to the instable solar and wind energy, geothermal energy is a more reliable renewable energy source, which makes people believe that geothermal energy can be the best alternative energy source for coal, natural gas and nuclear energy. In addition, geothermal energy is indeed an ideal clean energy source. It has abundant energy resources and does not generate greenhouse gases during extraction, which does not be harmful to the global environment.

There are three main types of geothermal power generation currently in use: (1) dry steam; (2) flash cycle [single flash cycle, double flash cycle, triple flash cycle]; (3) binary cycle. Besides above three types, there are other 4 geothermal power generation types, they are (4) Hot spring power generation; (5) Hot dry rock geothermal power [Enhanced Geothermal System; EGS]; (6) Magma power generation; (7) Back pressure type and condensing type.

In addition, as a future technology, high-temperature rock power generation that can generate electricity without hot water or steam resources is also researching and developing every day.

Another, regarding the handling of steam after usage in a power generation turbine, the method that releasing it into the atmosphere is classified as the back pressure method, and the method that cooling the steam back to water and recycle to use is classified as the condensate method.

The first geothermal power plant in the world was tested on natural steam in Larderello, Italy, on July 4, 1904, and commercial power generation as a power plant began in 1913 (250 kW). In 1942, the total output reached 120,000 kW, but the power plant at that time was destroyed by the war. After the World War II, a new power plant was constructed. As of 2010, the power plant has a power generation capacity of 543

MW and an annual power generation of approximately 5 billion kWh, Supplying power comparable to a medium-scale thermal power plant and one nuclear power plant. The total global geothermal power generation capacity in 2005 was 8878.5MW. Geothermal power generation accounts for about 0.3% of total power generation facilities around the world.

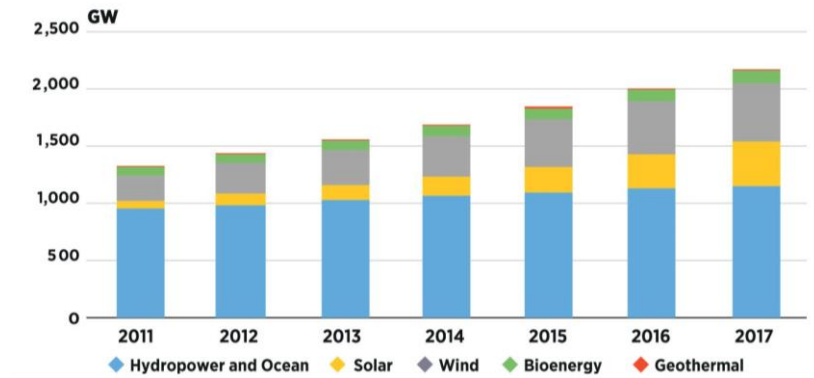


Figure 2. Total Renewable Power Generation Capacity, 2011-2017 from IRENA



Figure 3. Geothermal Power Generation and Cumulative Capacity by Region, 2017-2023 by IEA

Here, what we focus is the [Dry hot rock power generation system]. The idea of using underground hot dry rock to generate electricity was proposed by Americans Morton and Smith in 1970. In 1972, they drove two 4000m deep inclined wells in northern New Mexico, injecting cold water from one well into a dry and hot rock mass, and taking out steam generated from the heating of the rock mass from another well, with a power of 2300 kilowatts. Nowadays, Japan, the United Kingdom, France, Germany, and Russia have also done research on dry hot rock power generation, but no large-scale application and commercial project has been made so far.

1.3 Existent Difficulties in Popularizing Geothermal

1.3.1 Initial Cost

Compared with solar energy and wind energy, the use of geothermal energy is not limited by weather conditions. Although exploration and mining require professional technical support to avoid risks. Actually the initial cost of geothermal power plant construction is relatively high, but the cost consumed during operation is far lower than solar energy and wind energy. And geothermal has better stability and efficiency when operated, even general geothermal projects can recover costs within a few years.

In general, the initial cost of geothermal power generation will require from 7,000 dollars / kW to 11,000 dollars / kW or more just for the construction cost of power generation facilities. Design output facilities that generated electrical energy less than 15,000 kW will lead to expensive initial cost, and there have been existed cases which initial costs are up to 166 million dollars are required. If the amount of power generated exceeds 15,000 kW, the unit cost will be relatively low, but it will still cost about 110 million dollars in initial costs.

In addition, a considerable amount of preliminary survey costs and boring costs must be added, and as a result of the construction period is usually longer than several years, thus it must be not taken a considerable amount of time until starting operation. The long-term return of geothermal power is generally calculated to be 12-14%. In the case of photovoltaic power generation, it is considered to be about 6-7%, so the yield is quite high. However, this estimated yield can be maintained depends on whether the cost can be reduced with a short purchase guarantee period of 15 years or not. The initial cost of advanced excavation work must be kept at a low level by making full use of national subsidies.

Geothermal power generation has a tremendous initial investment amount, but due to weak power generation output and low thermal efficiency, we cannot expect a sufficient amount of power generation or investment effect in a short period of time. The big disadvantage is that the amount of investment is so large that it is difficult for individual investors to involve, and it is also difficult to introduce without sufficient funds even for rich corporates. If someone is planning to invest in geothermal power, make sure to consider not only the benefits of geothermal power but also the cost.

1.3.2 Environment concerns

Various environmental impacts can occur during operation of a geothermal plant. Geothermal fluids such as hot water and steam generally contain gas components such as carbon dioxide (CO₂), hydrogen sulfide (H₂S), ammonia (NH₃), methane (CH₄). And chemical components whose solubility increases with temperature, for example, sodium chloride (NaCl), boron (B), arsenic (As), mercury (Hg), etc. They will bring pollution if released into the environment. Although there has been geothermal fluid used for district heating in Iceland which is closed to fresh water, this is just a special case. On the other hand, the temperature of the wastewater produced by geothermal plant is often higher than the surrounding water temperature, which may cause thermal wastewater pollution. If the hot water used contains high concentrations of boron, fluorine compounds, arsenic, etc., it must be reduced underground after treatment.

Ground subsidence may occur along with normal groundwater pumping if a large amount of hot water is extracted from the underground. It takes several years until subsidence phenomenon becomes apparent, because land subsidence progresses slowly over a relatively wide area. Besides subsidence, in some areas, removing or returning hot water can cause earthquakes or increase the frequency of earthquakes. However, the magnitude of these earthquakes is usually very small and can only be detected by a highly sensitive seismometer. It is believed that geothermal use will not trigger a large earthquake, and in fact, there has never been such a serious example happened.

As conclusion, the main effects of geothermal power generation on the environment states on the following points:

- (1) Hot spring depletion: Hot spring resources are reduced or depleted by pumping;
- (2) Cliffs: Changes due to pumping up or reduction of waste water (returning to the ground);
- (3) Earthquake: An earthquake is triggered by pumping up or reducing unused water;
- (4) Groundwater contamination: Toxic substances dissolved in groundwater which is contaminated by reducing wastewater;
- (5) Air pollution: Air is polluted by toxic vaporizable substances;
- (6) Contamination of surface soil: The earth is polluted by toxic vaporizable substances and solid substances.

There are four main factors that cause above problems:

- (1) Pumping of hot water;
- (2) Reduction of waste water;
- (3) Toxicity in hot water and steam;
- (4) Facility construction itself.

1.3.3 Induced Seismic Activity

As mentioned above, seismic occurs at somewhere when satisfy specified conditions. Recently, something about earthquake induced by geothermal is the magnitude 5.4 Richter scale earthquake on November 15th, 2017 in Pohang may have been caused by an experimental geothermal power plant, reported by an investigation team from Korean media. This earthquake is the second largest earthquake in South Korea and the most destructive earthquake in modern Korean history, injuring 135 people and an estimated economic loss of 255 million dollars.

Unlike traditional geothermal power plants that extract energy directly from hot water or rocks underground. A type of Enhanced Geothermal System technology ---- Pohang Power Plant injects fluids into the ground under high pressure, breaking the rocks and releasing heat. The team found that this pressure triggered a small earthquake that affected nearby faults, eventually triggering a larger earthquake in 2017.

In order to explain the cause and effect of induced earthquake, here we use the magnitude 5.4 Richter scale earthquake on 2017 in Pohang as a sample. Geophysicist William Ellsworth (Stanford University) and Kang-Kun Lee (Seoul National University) and others published an article in Science on May 24, stating the culprit that caused the Pohang earthquake for the failure of the Pohang project and pointing out the development and utilization of geothermal resources. The seismic activity caused by the reservoir excitation activated the previously unknown faults and eventually triggered the main earthquake. The occurrence of the Pohang earthquake proved that EGS stimulation can cause large earthquakes beyond the stimulated volume, thus overturned the assumption that the maximum seismic magnitude is controlled by the volume of injected fluid. Many geothermal, oil and gas projects are also guided by the assumption that as long as the fluid injected into the well does not exceed a certain volume, the earthquake will not exceed a certain scale. But Pohang's experience tells us that this is not all. With this in mind, many projects are managed using so-called "Traffic Light Systems". As long as the earthquake is small, it can be turned on the green light and permitted to implement. If the earthquake starts to get bigger, adjustments can be made to continue the project. However, if the earthquake is too big, a red light will be turned on and the project will be stopped, at least temporarily.

In Pohang, water injection causes cracks in the rocks to form channels for absorbing

heat from the ground as similar with other enhanced geothermal projects ; otherwise, underground heat cannot be exploited for power generation with such low permeability. Ellsworth explained why Pohang project failed and analyzed how to reduce risks. This is not only related to subsequent geothermal power plants, but also to all hydraulic fracturing projects that require similar technologies. On the other hand, he said that despite these risks exist, it is still believed that enhanced geothermal systems can play an important role in renewable energy. Understanding Pohang's problems can allow other countries or regions to more safely develop and utilize dry hot rock geothermal resources effectively. It is known hydrothermal geothermal energy is relatively rare., the application of these resources will be unsustainable without good recharge measurement. If we can find a better method for safe power generation based on enhanced geothermal systems, it could bring us huge benefits and become the best choice for the issues of low-carbon economy and power generation.

In recent years, small earthquakes caused by the European EGS project during the drilling or production phase exceeded pre-set safety thresholds, leading to the termination of these projects. The problems of hydraulic fracturing and wastewater recharge during the development of oil and gas resources will also induce earthquakes. Although none of these earthquakes is as large as in Pohang in these cases, it will also cause local damage.

In the future EGS project, the project team and relevant scientific research institutions should conduct comprehensive and continuous monitoring and analysis of the evolving earthquake disasters in order to make the greatest contribution to mitigating the earthquake risk and the changing seismic risk situation Update information to government authorities. At the same time, further work is needed to establish physical and statistical models that induce and trigger seismic activity in order to provide a theoretical basis for risk assessment.

1.3.4 Relative Technology Development

There are many reasons that producing fluid directly from liquid-dominated geothermal systems is problematic:

- (1) The produced fluid may contain dissolved chemical components from the rock making it corrosive to the well and surface collection pipes;
- (2) Produced fluid may transport chemical species (e.g., acid gases) from the reservoir to the surface where they must be handled as hazardous pollutants;
- (3) The produced fluid itself may be hazardous and require special handling or incur disposal costs;
- (4) Injected working fluid may react with the rock and lead to formation damage, either excessively dissolving the reservoir or plugging it up;
- (5) There may not be sufficient permeability in the geothermal reservoir to inject or recover working fluid at sufficient rates.

Therefore, in order to avoid these problems is to keep reservoir fluids isolated from the geothermal energy recovery infrastructure through the use of a closed-loop circulation system in which the working fluid never contacts the host rock. On the other hands, unlike working fluid leakage in open system, it is sure that the amount of working fluid can be extracted with a stable rate.

Closed-loop system method has been proposed in the past, but limited to former technology and energy construction. However, due to recent developments in reservoir stimulation, drilling technology, and the use of novel working fluids, coupled with the imperative to lower environmental impacts of geothermal energy, are inspiring renewed interest in closed-loop systems.

Geothermal energy is the world's largest source of continuous clean power, but only 2% has been accessible. Conventional "open loop" geothermal power technology cannot access the hot dry rock regions where most geothermal power resides. Further, conventional geothermal technology requires high risk, fixed-scale power projects that require up to several years to plan and build. It is very unfriendly for investors and geothermal supported governments. Therefore, to address those problems, GreenFire Energy has developed its patented Green-Loop technology to generate continuous, cost competitive, and scalable geothermal power. GreenFire Energy uses advanced drilling

and well completion technology that revolutionized the oil and gas industry to maximize heat transport from deep in the earth to the surface. Green-Loop technology is the most environmentally attractive way of providing large scale renewable power generation.

GreenFire Energy's advanced ECO2G™ technology extracts geothermal energy unavailable to conventional systems and provides cost competitive, stable, and reliable power. The company designs, develops, and builds projects that use a patented closed-loop architecture to capture heat energy from marginal conventional wells and, eventually, large-scale greenfield projects. The GreenFire Energy then retained **Baker Hughes** to help build a drilling cost model to determine the economic viability of ECO2G in a wide variety of conditions. More recently, GreenFire and partners at the Lawrence Livermore National Laboratory were awarded funding under the Department of Energy's Small Business Voucher program. LBNL will perform research related to novel methods of well completion and directional drilling in hot and deep geothermal formations.

1.4 Enhanced Geothermal System (EGS)

1.4.1 What is EGS ?

In geothermal power generation, it is a technology that feeds working fluid and obtains steam or hot water in poor natural hot water or steam circumstance. EGS injects water into underground to hydraulically crush hot rock with low permeability, then water becomes steam and hot water are obtained by means of creating a water reservoir. It is expected the EGS technology could expand geothermal utilization opportunities all over the world. As to the utilization of the produced steam (heat energy) in EGS. It is as similar that the method of electric power, which is obtained by turning the steam turbine of the generator forced by steam generated mainly through geothermal heat, as in the case of conventional geothermal power generation.

Geothermal energy is one of the power generation which is not derived from the sun. It has been pointed out that the current technology could reduce the cost until 0.08 dollar / kWh. In 2008, Google invested 10 million dollars in venture companies and became a popular topic. On the other hand, “Induction of earthquake” and “Difficulty in securing injected water” have been pointed out as main issues. In the case of Basel, Switzerland, an earthquake was triggered by water injection, which caused property damage up to \$ 9 million. Therefore, the project was canceled and the president of the development corporation was prosecuted and even brought to trial. The recovery rate of injected water is said to have an impact on practical operation unless it is over 80%.

EGS demonstration experiments are implemented at some countries, we will make use of our hot rock power generation technology (see figure 4, 5) and establish EGS technology, which will contribute to the reduction of geothermal development risk and power generation cost.

In figure 4., when natural hot water supply (rainwater) is insufficient, surface water is supplied from other wells to the reservoir. But in figure 5., the steam production will be increased by increasing the water permeability of the rock mass around the production well due to hydraulic fracturing from the production well and other wells. Currently, in figure 6., a reservoir which is created artificially by hydraulic fracturing from a drilling well, and then water injected from the surface is produced from production wellbore as hot water or steam.

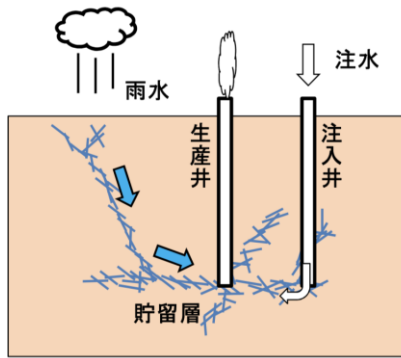


Figure 4. Reservoir recharge EGS concept

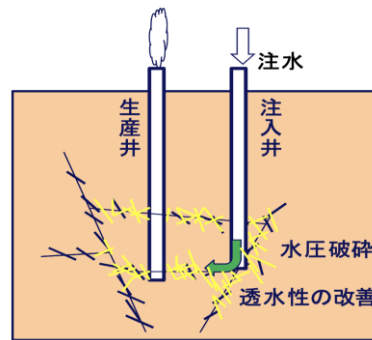


Figure 5. Water permeability improvement EGS concept

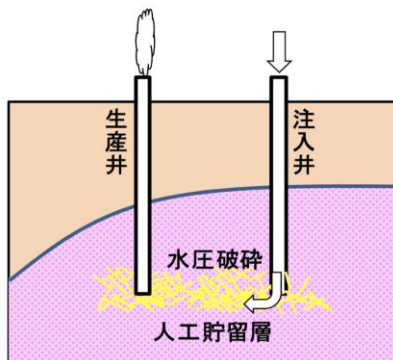


Figure 6. Reservoir creation EGS concept

——電力中央研究所報告 「地熱増産システム(EGS)技術開発の現状と課題」

Over the next 20 years, prospect of commercialization in the demonstration plant of EGS will be set up. At the same time, conventional geothermal development will be carried out in parallel. In addition, a wider scale of geothermal energy must be considered, including the heat resource at every depth, low, medium and high temperature geothermal resources that have not been used.

From now on, widely disseminate know-how on EGS technology to improve productivity, resource sustainability and improve health, safety and environmental management skills is more and more necessary. Geothermal utilization and power generation are easy to develop in the many areas of developing countries. The reason why is that it is easy to overcome the economic and non-economic barriers against development. Therefore, geothermal (EGS) may be most attractive energy generation resources available to those developing countries.

1.4.2 Advantages of Using CO₂ as Working Fluid

It aims at creating geothermal field by circulating water through hot rocks at deep underground. The power output efficiency is not good because current technology is still immature in the preliminary stage. For the purpose of high energy efficiency, we choose a new working fluid. Here, we are using supercritical carbon dioxide (SCCO₂) instead of water as the circulating fluid, and trying to increase the efficiency up to three times than conventional ones.

A supercritical fluid is a state that has properties between liquid and gas. It shows no surface tension even when released as a gas. The CO₂ pressure-temperature phase diagram is shown in Figure 7. T_c is the critical temperature and P_c is the critical pressure. Supercritical carbon dioxide (SCCO₂) has a very low viscosity and high buoyancy, which can significantly reduce the energy pumped cost compared to what spent with water. In addition, supercritical fluids have a high heat extraction rate and are unlikely to melt rock in the reservoir.

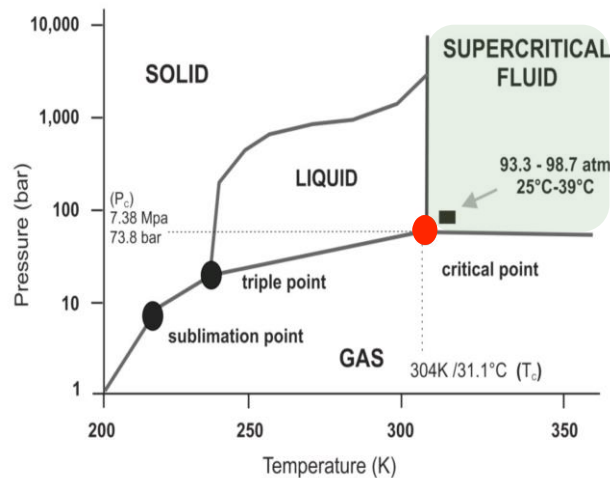


Figure 7. CO₂ pressure-temperature phase diagram

CO₂ has properties between fluid and gas in the supercritical region. In this region, a small increase in pressure will result in a significant increase in density. At present, critical CO₂ is also used in dry cleaning of fabrics as an alternative to conventional chlorinated solvents which is extremely harmful to the ozone layer. It is also used to extract aroma from spices and caffeine from coffee. As it rises toward the surface due to the buoyancy of CO₂, the temperature and pressure of SCCO₂ decreases, changes to

a liquid state, and dissolves into the pore water of the rock. Some of the CO₂ crystallizes into calcite, effectively forming a lid on the supercritical portion of the reservoir.

In any geothermal circulation scheme, to some extent rocks, cracks, unbonded gaps and other general imperfections cause the fluid to escape into the formation when pumping fluid. Because the time that the fluid contacts the rock could be maximized, connected rock fissures form a dense network will be formed, that is the meaning of an ideal reservoir. One of the advantages of using CO₂ as a working fluid is that it works for those with better loss in the formation as described above. The reason why is carbon sequestration is becoming a partial solution to greenhouse gas emissions.

1.4.3 Current state of EGS development

As one of conventional geothermal methods, EGS is limited to moderate temperature zones where there is sufficient permeability for water to flow to production wells and so is limited to use only about 2% of the available geothermal resource. As competing technology in using geothermal power, EGS has tried for decades to create artificial permeability. However, EGS is still far from commercialization because of the difficulty of creating long symmetrical cracks in complex and varied terrains.

ECO₂G is an environmentally advanced renewable power technology designed to access the vast unexploited geothermal resources located around the world. Lack of subsurface permeability has been the greatest constraint for conventional hydrothermal projects. To circumvent the permeability problem, ECO₂G circulates SCCO₂ in a closed-loop pipe system to gather and transfer high temperature heat.

Compared with EGS (open system), ECO₂G uses oil and gas drilling technology to create closed-loop sealed wells. Further, SCCO₂ is better than water for heat transfer in this system, and thus eliminates the water constraint. This simplified approach reduces the complexity and risk of drilling, thus transforming geothermal development from a series of wildcatting ventures into an industrial process.

Chapter 2: Methodology

2.1 Introduction

TOUGH2 is a numerical simulator for non-isothermal flows of multicomponent, multiphase fluids in 1, 2, and 3-dimensional porous and fractured media. The main applications for which TOUGH2 is developed are in geothermal reservoir engineering, nuclear waste disposal, environmental assessment and remediation, and unsaturated and saturated zone hydrology. TOUGH2 was first released to the public in 1991; the 1991 code was updated in 1994 when a set of preconditioned conjugate gradient solvers was added to allow a more efficient solution of large problems.

TOUGH2 can solve not only mass and energy balance equations that describe fluid and heat flow in general multiphase, but also multicomponent systems (Appendix A). Fluid advection is described with a multiphase extension of Darcy's law; additionally, there is diffusive mass transport in all phases. Heat flow occurs by conduction and convection, the latter including sensible as well as latent heat effects. The description of thermodynamic conditions is based on the assumption of local equilibrium of all phases. Fluid and formation parameters can be arbitrary nonlinear functions of the primary thermodynamic variables.

For (1) better understanding of borehole-flow and (2) transport processes and (3) improving the design of injection operations, Lawrence Berkeley National Laboratory (LBNL) have developed a borehole-flow simulator for CO₂ and variable salinity water that models transient non-isothermal processes involved with the flow of CO₂ in deep boreholes and wells including transitions from supercritical to gaseous phases. According to T2Well/ECO2N Manual, the new wellbore flow model is based on the drift-flux model (DFM) approach and is an extension of TOUGH2/ECO2N, which can describe single- and two-phase flows of CO₂-water-NaCl mixtures but cannot describe three-phase conditions that would include a situation where both liquid and gaseous CO₂-rich phases coexist. Unlike the earlier coupling approach, the deliver-ability option in TOUGH2 is not used and the flow in the wellbore is not assumed to be at steady state. Alternatively, the T2Well/ECO2N is an integrated simulator of a wellbore-reservoir

system of CO₂-brine in which the wellbore and reservoir are two different sub-domains where flow is controlled by different physical laws.

As mentioned above, the approach LBNL use for describing wellbore flow is based on the drift-flux model (DFM) for 1-dimensional transient 2-phase non-isothermal flow of CO₂-water mixtures. Conservation equations for mass, momentum and energy under different flow regimes in the wellbore are solved numerically while heat transmission from the wellbore to the surrounding rock is either handled semi-analytically or numerically. LBNL implement the DFM in TOUGH2 with the ECO2N equation of state module. As to the conventional approach for calculating the mixture velocity in the drift- flux model (DFM), is often based on the steady-state pressure loss equation for wellbore flow. Therefore, in order to improve simulation performance in wellbore flow processes involving high fluxes, LBNL have extended the DFM to include the transient terms of the momentum conservation equations in calculating the velocity from the pressure gradient.

The accuracy of T2Well must be considered, LNBL has been tested by comparison with many different analytical and numerical solutions, with results from laboratory experiments, and with field observations. However, it should be emphasized that the integration of many different modules into a single program structure is a difficult and potentially “tough task”. Many different options can be selected in different program modules.

2.2 Mathematical Formulation

2.2.1 Mass and Energy Conservation Equations

According to the manual of T2Well/ECO2N Version 1.0 (Multiphase and Non-Isothermal Model for Coupled Wellbore-Reservoir Flow of Carbon Dioxide and Variable Salinity Water), based on mass and energy conservation principles, the generalized conservation equation of mass components and energy in wellbore governed by T2Well can be written as follows:

$$\frac{\partial M^\kappa}{\partial t} = q^\kappa + F^\kappa \quad (1)$$

Where superscript κ is the index for the components, $\kappa = 1$ means H₂O, 2 means CO₂, and 3 (energy, included internal and kinetic energy), M^κ are the accumulation terms of the components κ , q^κ are source/sink terms for mass or energy components; and F^κ are the mass or energy transport terms along the borehole due to advective processes.

The accumulation term M^κ of Eq. (1) for the mass components (H₂O, CO₂) in single- or two- phase system is given by

$$M^k = \rho_G S_G X_G^k + \rho_L S_L X_L^k \quad (k = 1 \text{ and } 2) \quad (2)$$

Where X_β^k is the mass fraction of component κ in fluid phase β ($\beta = G$ means gas; $\beta = L$ means liquid), ρ_β is the density of phase β ; and S_β is the local saturation of phase β defined as

$$S_G = \frac{A_G}{A} = \frac{A_G}{A_G + A_L} \quad (3)$$

Where A is the well cross-sectional area; A_G and A_L denote the cross-sectional areas occupied by gas and liquid over the cross section at a given elevation. And the accumulation term for energy is defined as

$$M^3 = \sum_\beta \rho_\beta S_\beta \left(U_\beta + \frac{1}{2} u_\beta^2 \right) \quad (4)$$

Where u_β is the internal energy of phase β per unit mass and $\frac{1}{2}u_\beta^2$ is the kinetic energy per unit mass while u_β is the velocity of phase β in the wellbore.

It is known that working fluid transport along the wellbore is governed by processes of advection, diffusion, and dispersion, and is also subject to other processes, for example, exchanges with the formation at feed or thief zones. The total advective mass transport term for component κ can be written in one- dimension as

$$F^k = -\frac{1}{A} \left[\frac{\partial(A\rho_G X_G^k S_G u_G)}{\partial z} + \frac{\partial(A\rho_L X_L^k S_L u_L)}{\partial z} \right] \quad (5)$$

Where u_β is the average velocity vector of phase within the wellbore, A is the cross-sectional area of wellbore, and z is the coordinate along the wellbore (vertical, inclined, or horizontal). The transport terms for energy in the wellbore include follow activities: (1) advection, (2) kinetic energy, (3) potential energy, and (4) lateral wellbore heat loss/gain. The overall one-dimensional energy transport term can be written as

$$F^3 = -\lambda \frac{\partial T}{\partial z} - \frac{1}{A} \sum_{\beta} \frac{\partial}{\partial z} \left[A \rho_{\beta} S_{\beta} u_{\beta} \left(h_{\beta} + \frac{u_{\beta}^2}{2} \right) \right] - \sum_{\beta} (S_{\beta} \rho_{\beta} u_{\beta} g \cos \theta) - q'' \quad (6)$$

Where h_{β} is specific enthalpy of fluid phase β , θ is the incline angle of the wellbore, g is the gravitational acceleration, q'' is the wellbore heat loss/gain per unit length of wellbore, and ρ_m is the density of the gas-liquid mixture. T is the temperature, and λ is the average value of thermal conductivity of the wellbore (both phases of the fluids and solid).

Pay attention to that the mass or energy exchange terms between a perforated wellbore section and its surrounding formation are omitted from the above equations for simplicity. These terms in above equations are calculated as flow through porous media as implemented in normal TOUGH2 except that the nodal distance to the interface on the wellbore side is set to zero in the grid.

2.2.2 Momentum Conservation (Drift-Flux Model)

In contrast to flow through porous media in which the flux or the velocity can be simply determined from the gradient of pressure and gravity using Darcy's Law, the determination of flow velocity in a wellbore involves solving the appropriate momentum conservation equations. In fact, directly solving the momentum equations of two phase flow is really difficult and often not practical as it has to be coupled into another reservoir simulator. Therefore, LNBL invoke the Drift Flux Model (DFM) to describe both single-phase and multiphase flow in wellbores to obtain the advective transport terms (F_β , u_β).

Next, the drift-flux model is limited to one dimensional flow through an open pipe or annulus. Therefore, all variables in the development below should be considered as area-averaged or assumed to be constant over the cross-section except for those explicitly noted otherwise. It is said that the DFM were first developed by Findlay (1965) and Wallis (1969). Although various nomenclatures and forms of equations were used to describe the DFM in the literature over decades, the basic idea of the DFM is to assume that the gas velocity--- u_G , can be related to the volumetric flux of the mixture--- j , and the drift velocity of gas--- u_d , by the following empirical constitutive relationship:

$$u_G = C_0 j + u_d \quad (7)$$

Where C_0 is the profile parameter to account for the effect of local gas saturation and velocity profiles over the pipe cross-section. According to definition, the volumetric flux j is the volumetrically weighted velocity

$$j = S_G u_G + (1 - S_G) u_L \quad (8)$$

For this reason, we can determine the liquid velocity u_L as

$$u_L = \frac{1 - S_G C_0}{1 - S_G} j - \frac{S_G}{1 - S_G} u_d \quad (9)$$

With the governing equations (7)(8)(9), LNBL simplified the momentum equations of two-phase flow in a wellbore into a single equation in terms of the mixture velocity u_m and the drift velocity u_d as follows:

$$\frac{\partial}{\partial t}(\rho_m u_m) + \frac{1}{A} \frac{\partial}{\partial z} [A(\rho_m u_m^2 + \gamma)] = -\frac{\partial P}{\partial z} - \frac{\Gamma f \rho_m |u_m| u_m}{2A} - \rho_m g \cos \theta \quad (10)$$

Where the term $\gamma = \frac{S_G}{1-S_G} \frac{\rho_G \rho_L \rho_m}{\rho_m^{*2}} [(C_0 - 1)u_m + u_d]^2$ is caused by slip between the two phases. The mixture density, ρ_m , and the mixture velocity (velocity of mass center), u_m , are defined as follows:

$$\rho_m = S_G \rho_G + (1 - S_G) \rho_L \quad (11)$$

and

$$u_m = \frac{S_G \rho_G u_G + (1 - S_G) \rho_L u_L}{\rho_m} \quad (12)$$

Then, the profile-adjusted average density is defined as follows:

$$\rho_m^* = S_G C_0 \rho_G + (1 - S_G C_0) \rho_L \quad (13)$$

Therefore, using the DFM approach to solve the complicated momentum equations of two-phase flow becomes an easier task with two steps. First step, LNBL obtain the mixture velocity by solving the simplified momentum Equation (10) and the drift velocity from some empirical relationships. Second step, LNBL calculate the gas velocity and the liquid velocity as a function of u_m and u_d as follows:

$$u_G = C_0 \frac{\rho_m}{\rho_m^*} u_m + \frac{\rho_L}{\rho_m^*} u_d$$

$$u_L = \frac{(1-S_G C_0) \rho_m}{(1-S_G) \rho_m^*} u_m - \frac{S_G \rho_G}{(1-S_G) \rho_m^*} u_d \quad (14)$$

In general, it's difficult to accurately estimate the drift velocity u_d and the profile parameter C_0 . Thus, DFM is the effort to try to solve calculate more accurately. As a result, such relationships have been proposed to describe by C_0 and u_d , they could be a function of flow regime and many other formulas. The following is a summary of the mathematical formulations related to the drift velocity proposed by Shi et al. (2005) who is the developer of DFM that are implemented in T2Well.

First of the summary, the drift velocity is calculated as a function of gas saturation and other fluid properties:

$$u_d = \frac{(1 - C_0 S_G) u_c K(S_G, K_u, C_0) m(\theta)}{C_0 S_G \sqrt{\rho_G / \rho_L} + 1 - C_0 S_G} \quad (15)$$

Where $m(\theta)$ describes the effect that inclination of the wellbore:

$$m(\theta) = m_0 (\cos \theta)^{n_1} (1 + \sin \theta)^{n_2} \quad (16)$$

Where m_0 , n_1 , n_2 are all fitted parameters.

K_u is the Kutateladze number, N_B is a function of Bond number:

$$K_u = \left[\frac{C_{ku}}{\sqrt{N_B}} \left(\sqrt{1 + \frac{N_B}{C_{ku}^2 C_w}} - 1 \right) \right]^{\frac{1}{2}} \quad (17)$$

Where C_w (in the T2Well code, C_w was assumed to be a constant of 0.008) is a wall friction factor and the Bond number is defined as:

$$N_B = d^2 \left[\frac{g(\rho_L - \rho_G)}{\sigma_{GL}} \right] \quad (18)$$

Where d is the wellbore diameter and C_{ku} was 75 in Richter's original formula, which resulted in overestimation of K_u in the range of smaller dimensionless diameter (Richter, 1981), is used in T2Well.

The “characteristic velocity”, u_c , is a measure of the velocity of bubble rise in a liquid column, given by

$$u_c = \left[\frac{g\sigma_{GL}(\rho_L - \rho_G)}{\rho_L^2} \right]^{\frac{1}{4}} \quad (19)$$

Where σ_{GL} is the surface tension between gas and liquid phases.

The function $K(\alpha)$ in Equation (16) is used to make a smooth transition of drift velocity between the bubble rise stage and the film flooding stage. Different from the linear interpolation suggested by Shi et al. (2005), LNBL use the following smooth function:

$$K = \begin{cases} 1.53 + \frac{C_0 K_u - 1.53}{2} \left[1 - \cos \left(\pi \frac{S_G - a_1}{a_2 - a_1} \right) \right] & S_G \leq a_1 \\ C_0 K_u & a_1 \leq S_G \leq a_2 \\ C_0 K_u & S_G \geq a_2 \end{cases} \quad (20)$$

Where a_1 and a_2 are two transition points of gas saturation as suggested by Shi et al. (2005). Because K is independent of the gas saturation for $S_G \leq a_1$ and $S_G \geq a_2$, the function K is constructed such that $dK/dS_G = 0$ in the neighborhoods of a_1 and a_2 , making this derivative continuous over the entire range of S_G . The fitting parameters, m_0 , n_1 , n_2 , a_1 , and a_2 are all hardwired in the code and the values are obtained from the case of water/gas in Shi et al. (2005) depending on C_{max} (a user-specified maximum profile parameter between 1.0 and 1.5) as follows:

Table 1. Empirical parameters of DFM used in T2Well.

Fitting Parameter	Value for $C_{max} = 1.0$	Value for $C_{max} = 1.2$
a_1	0.06	0.06
a_2	0.21	0.12
m_0	1.85	1.27
n_1	0.21	0.24
n_2	0.95	1.08

Source: Shi et al., 2005.

Second of summary, the profile parameter C_0 is calculated using the same formulas suggested by Shi et al. (2005) as listed below (with different symbols) for completeness:

$$C_0 = \frac{C_{max}}{1 + (C_{max} - 1)\eta^2} \quad (21)$$

Where η is a parameter reflecting the effects of the flow status on the profile parameter and is calculated as follows:

$$\eta = \frac{\beta - B}{1 - B} \quad (0 \leq \beta \leq 1) \quad (22)$$

Where B is the threshold parameter above which C_0 starts to drop below C_{max} and β is calculated as follows:

$$\beta = \max[S_G, F_V \frac{S_G |u_m|}{u_{sgf}}] \quad (23)$$

Slightly different from Shi et al. (2005), LNBL tied the threshold parameter B as a function of C_{max} :

$$B = \frac{2}{C_{max}} - 1.0667 \quad (24)$$

Equation (25) provides $B = 0.6$ for $C_{max} = 1.2$, which is consistent with the values of ($a_1=0.06$) and ($a_2=0.12$) (Shi et al., 2005). B varies from 0.9333 ($C_{max} = 1.0$) to 0.2666 ($C_{max} = 1.5$). Note that if $C_{max} = 1.0$ (the optimal value for water/gas system as suggested by Shi et al., 2005), C_0 would be independent of gas saturation or velocity and the profile effect disappears.

Profile flattening can be made more or less sensitive to the gas velocity by adjusting the value of F_V (default =1) in Equation (23) whereas the “flooding” gas superficial velocity, u_{sgf} , is calculated as follows:

$$u_{sgf} = K_u \left(\frac{\rho_L}{\rho_G} \right)^{\frac{1}{2}} u_c \quad (25)$$

2.2.3 Discretized Equations

As an extension to standard TOUGH2/ECO2N, T2Well has the same framework with TOUGH2, when the mass and energy flux terms are calculated at each Newtonian iteration from the most recently updated primary variables (usually pressure, mass fractions, and temperature). At each iteration in the wellbores, LNBL calculate the mixture velocity (Eq. 10) first, then calculate drift velocity (Eq. 15) and finally calculate the gas velocity and the liquid velocity (Eq. 14). As for marching in time, the momentum conservation equation (Eq. 10) is solved semi-explicitly at interfaces of the neighbouring wellbore cells as

$$u_m^{n+1} = \frac{DR^{n+1} + \frac{1}{\Delta t} \rho_m^n u_m^n - \left[\frac{1}{A} \frac{\partial}{\partial z} (A \sum_{\beta} \rho_{\beta} S_{\beta} u_{\beta}^2) \right]^n}{\frac{\rho_m^{n+1}}{\Delta t} + \frac{f^n \Gamma \rho_m^{n+1} |u_m^n|}{2A}} \quad (26)$$

At Eq. 26, the superscripts n and $n+1$ denote the previous and current time steps, respectively; Δt is the time-step size, and DR is the total driving force given by

$$DR = -\frac{\partial P}{\partial z} - \rho_m g \cos \theta \quad (27)$$

Commonly, there are many reasons caused pressure loss, such as elevation change which contributes from 80% to 95%, and the friction represents 5% to 20%, however the acceleration loss is usually negligible and can become significant only if a compressible phase happens at relatively low pressures (Brill, 1999) or DR becomes very small (e.g., near hydrostatic state). Therefore, this method is more similar to the implicit formula considering the normal pressure loss partition described above. Here, because the spatial acceleration term is entered as an explicit term in the equation, the original formula of the sum of two additions can be used directly, regardless of the mixture velocity and an additional term due to drift velocity. If the change of spatial acceleration over Δt is negligible compared to the driving force, Eq. 26 should provide an accurate solution for Eq. 10. When the system reaches steady state, the solution is an exact numerical solution of the Eq. 10 and the accuracy depends only on grid resolution.

Mass and energy balance equations for the components of Eq. 1 are discretized in space using the traditional integrated finite difference scheme of TOUGH2 for well system. Apart from the special treatment of the momentum equation (Eq. 26), the time discretization is performed using an inverse first-order fully implicit finite difference scheme. Discrete nonlinear equations for H₂O, CO₂, and energy conservation at node *i* (well block) can be described in general form:

$$\left[M_i^{\kappa,n+1} - M_i^{\kappa,n} \right] \frac{V_i}{\Delta t} = F_{i,i+1/2}^{\kappa,n+1} - F_{i,i-1/2}^{\kappa,n+1} + Q_i^{\kappa,n+1} \quad (\kappa = 1, 2, \text{ and } 3) \quad (28)$$

Where the superscript *n* indicates the previous time level, and *n* + 1 is the current time level to be resolved. The subscript *i* refers to the index of wellbore grid cell; Δt is the time step size. V_i is the volume of wellbore cell *i* (wellbore diameter may vary). Flows terms in Eq. 28 are general and involves mass fluxes and heat transfer through both phases. The mass flow term is

$$F_{ij}^{\kappa} = A_{ij \Sigma_{\beta}} (\rho_{\beta} S_{\beta} X_{\beta}^{\kappa})_{ij+1/2} u_{\beta,ij} \quad (29)$$

The total heat flux along the connection of nodes *i* and *j* may be estimated by

$$F_{ij}^3 = A_{ij} \left\{ -\lambda \frac{\partial T}{\partial z} + \sum_{\beta} \left[(\rho_{\beta} S_{\beta} (h_{\beta} + \frac{u_{\beta}^2}{2}))_{ij+1/2} u_{\beta,ij} \right] \right\} \quad (30)$$

Where λ is the area-averaged thermal conductivity of the wellbore (both phases of the fluids and possible solid portion).

The heat exchange between the wellbore and the surrounding formation is calculated as the "normal" heat flow term in standard TOUGH2 if the surrounding formation is explicitly represented by a numerical grid, or Calculated (optionally) semi-analytically if there is a grid block of surrounding formation. In the latter case, Q_i^3 , which includes both heat loss/gain due to heat transfer in the horizontal well and

potential energy gain (friction energy loss converts to heat and does not affect the overall energy balance) are described by

$$Q_i^3 = -A_{wi}(K_{wi}) \left[\frac{T_i - T_\infty(z)}{r f(t)} \right] + \sum_{\beta} (\rho_{\beta} u_{\beta} g \cos \theta)_i \quad (31)$$

A_{wi} is the lateral area between the wellbore and the surrounding formation; K_{wi} is the thermal conductivity (or overall heat transfer coefficient) of the wellbore/formation. T_i is the temperature of the i th wellbore node and $T_\infty(z)$ is the ambient temperature; r is the wellbore's radius and $f(t)$ is Ramey's heat loss function (Ramey 1962):

$$f(t) = \frac{1}{-\ln\left(\frac{r}{2\sqrt{\alpha t}}\right) - 0.29} \quad (32)$$

Where α is the thermal dispersion of the surrounding stratum. The term u_i is the nodal velocity obtained by averaging the velocity at the interfaces. Second term of Eq. 31 reflects the net energy gain or loss per unit time due to gravity and is calculated as a sum of the net potential energy gain rate in both phases of grid cell i . Again, for simplicity, the above equations omit the specified energy source/sink terms, or the mass/energy exchange terms between the perforated well and the surrounding formation.

When evaluating the flow term from Eq.29 to Eq. 31, the subscript $ij+1/2$ is used to indicate an appropriate average or weighting of the advection mass transport or heat transfer characteristics along the interface or connection between two blocks or nodes i and j ($j = i-1$ or $i+1$). In addition, the Eq.29 and Eq.20 must use completely upstream weights for numerical stability. In a leaking/supplying zone of the wellbore, the mass or energy inflow/outflow terms are calculated as in standard TOUGH2 (i.e., flow through porous media).

The standard TOUGH2 fully implicit residual-based method is used to solve discrete nonlinear equations using Newton iteration. In general, it's needed to solve four major variables of ECO2N (pressure, saturation, or mass fraction of H₂O, CO₂, and NaCl in the fluids depending on phase conditions and temperature) at each node. The remaining variables, such as viscosities, densities, and thermal conductivities, etc. are secondary variables that can be calculated from the selected primary variables. Newton's iterative process continues until the residuals fall below a preset convergence level. The sparse Jacobi matrices generated by Newton's method are solved by the user-selected conjugate gradient provided by TOUGH2. The time step sizes tend to be much smaller than the TOUGH2 problems for typical all-porous media because of the higher flow rates and sensitivity to the time step size associated with wellbore flow. Besides the explicit spatial acceleration terms used in solving the momentum equation, all the velocities used in calculation of kinetic and potential energy in the energy balance equations are also explicit to avoid unnecessarily slow convergence.

2.3 Space and Time Discretization

The continuum Eq.33 are discretized in space using the integral finite difference method (IFD; Edwards, 1972; Narasimhan and Witherspoon, 1976). Introducing appropriate volume averages,

$$\int_{V_n} M dV = V_n M_n \quad (33)$$

Where M is a volume-normalized extensive quantity, and M_n is the average value of M over V_n . Surface integrals are approximated as a discrete sum of averages over surface segments A_{nm} :

$$\int_{\Gamma_n} \mathbf{F}^K \cdot \mathbf{n} d\Gamma = \sum_m A_{nm} F_{nm} \quad (34)$$

Where F_{nm} is the average value of the F (inner) normal component on the surface segment A_{nm} between the volume elements V_n and V_m . Figure 8 shows the discretization approach and the definition of the geometric parameters used in the integral finite difference method.

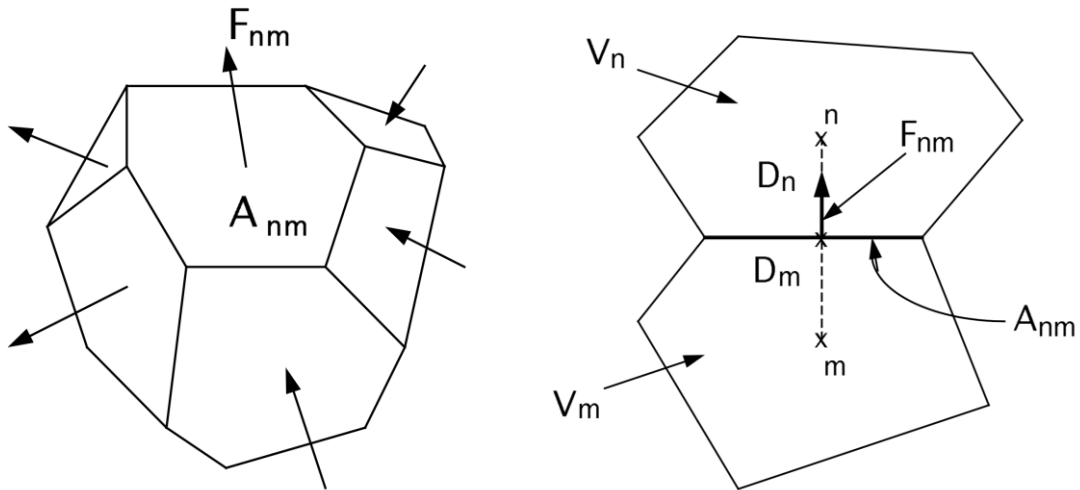


Figure 7. Space discretization and geometry data in the integral finite difference method.

The discretized flux is expressed in terms of averages over parameters for elements V_n and V_m . For the individual phase fluxes are given by a multiphase version of Darcy's law:

$$\mathbf{F}_\beta = \rho_\beta \mathbf{u}_\beta = -k \frac{k_{r\beta} \rho_\beta}{\mu_\beta} (\nabla P_\beta - \rho_\beta \mathbf{g}) \quad (35)$$

For the basic Darcy flux term LNBL uses

$$F_{\beta,nm} = -K_{nm} \left[\frac{k_{r\beta} \rho_\beta}{\mu_\beta} \right]_{nm} \left[\frac{P_{\beta,n} - P_{\beta,m}}{D_{nm}} - \rho_{\beta,nm} \mathbf{g}_{nm} \right] \quad (36)$$

Where the subscripts (nm) denote a suitable averaging at the interface between grid blocks n and m (interpolation, harmonic weighting, upstream weighting). $D_{nm} = D_n + D_m$ is the distance between the nodal points n and m , and \mathbf{g}_{nm} is the component of gravitational acceleration in the direction from m to n . Substituting Eq.33 and Eq.34 into the governing Eq.37, a set of first-order ordinary differential equations in time is obtained.

$$\frac{d}{dt} \int_{V_n} M^\kappa dV_n = \int_{\Gamma_n} \mathbf{F}^\kappa \cdot \mathbf{nd}\Gamma_n + \int_{V_n} q^\kappa dV_n \quad (37)$$

$$\frac{dM_n^\kappa}{dt} = \frac{1}{V_n} \sum_m A_{nm} F_{nm}^\kappa + q_n^\kappa \quad (38)$$

Time is discretized as a first-order finite difference, and the flux and sink and source terms on the right-hand side of Eq.38 are evaluated at the new time level, $t^{\kappa+1} = t^\kappa + \Delta t$, to obtain the numerical stability needed for an efficient calculation of multiphase flow. This treatment of flux terms is known as “fully implicit,” because the fluxes are expressed in terms of the unknown thermodynamic parameters at time level $t^{\kappa+1}$, so that these unknowns are only implicitly defined in the resulting equations (e.g., Peaceman, 1977). The time discretization results in the following set of coupled non-linear, algebraic equations

$$R_n^{\kappa,k+1} = M_n^{\kappa,K+1} - M_n^{\kappa,K} - \frac{\Delta t}{V_n} \{ \sum_m A_{nm} F_{nm}^{\kappa,K+1} + V_n q_n^{\kappa,K+1} \} = 0 \quad (39)$$

Where LNBL have introduced residuals $R_n^{\kappa,K+1}$. For each volume element (grid block) V_n , there are NEQ equations ($\kappa = 1, 2, \dots, \text{NEQ}$; usually, $\text{NEQ} = \text{NK} + 1$), so that for a flow system with NEL grid blocks (39) represents a total of $\text{NEL} \times \text{NEQ}$ coupled non-linear equations. The unknowns are the $\text{NEL} \times \text{NEQ}$ independent primary variables $\{x_i; i = 1, \dots, \text{NEL} \times \text{NEQ}\}$ which completely define the state of the flow system at time level t^{K+1} . These equations are solved by Newton/Raphson iteration, which is implemented as follows. We introduce an iteration index p and expand the residuals $R_n^{\kappa,K+1}$ in Eq. 39 at iteration step $p+1$ in a Taylor series in terms of those at index p .

$$R_n^{\kappa,k+1}(x_i, p+1) = R_n^{\kappa,K+1}(x_{i,p}) + \sum_i \frac{\partial R_n^{\kappa,k+1}}{\partial x_i} \Big|_p (x_{i,p+1} - x_{i,p}) + \dots = 0 \quad (40)$$

Retaining only terms up to first order, LNBL obtain a set of $\text{NEL} \times \text{NEQ}$ linear equations for the increments $(x_{i,p+1} - x_{i,p})$:

$$- \sum_i \frac{\partial R_n^{\kappa,K+1}}{\partial x_i} \Big|_p (x_{i,p+1} - x_{i,p}) = R_n^{\kappa,K+1}(x_{i,p}) \quad (41)$$

All terms $\partial R_n / \partial x_i$ in the Jacobian matrix are evaluated by numerical differentiation. Eq. 41 is solved by sparse direct matrix methods (Duff, 1977) or iteratively by means of preconditioned conjugate gradients (Moridis and Pruess, 1995, 1998). Iteration is continued until the residuals $R_n^{\kappa,K+1}$ are reduced below a preset convergence tolerance.

$$\left| \frac{R_{n,p+1}^{\kappa,k+1}}{M_{n,p+1}^{\kappa,k+1}} \right| \leq \varepsilon_1 \quad (42)$$

The default (relative) convergence criterion is $\varepsilon_1=10^{-5}$ (TOUGH2 input parameter RE1). When the accumulation terms are smaller than ε_2 (TOUGH2 input parameter RE2, default $\varepsilon_2 = 1$), an absolute convergence criterion is imposed,

$$|R_n^{K,K+1}| \leq \varepsilon_1 \cdot \varepsilon_2 \quad (43)$$

Convergence is usually attained in 3 ~ 4 iterations. If convergence cannot be achieved within a certain number of iterations (default 8), the time step size Δt is reduced and a new iteration process is started.

It is appropriate to add some comments about our space discretization technique. The entire geometric information of the space discretization in Eq. 39 is provided in the form of a list of grid block volumes V_n , interface areas A_{nm} , nodal distances D_{nm} and components g_{nm} of gravitational acceleration along nodal lines. There is no reference whatsoever to a global system of coordinates, or to the dimensionality of a particular flow problem. The discretized equations are in fact valid for arbitrary irregular discretizations in one, two or three dimensions, and for porous as well as for fractured media. This flexibility should be used with caution, however, because the accuracy of solutions depends upon the accuracy with which the various interface parameters in equations such as Eq.37 can be expressed in terms of average conditions in grid blocks. A general requirement is that there exists approximate thermodynamic equilibrium in almost all grid blocks at almost all times (Pruess and Narasimhan, 1985). For systems of regular grid blocks referenced to global coordinates (such as r-z, x-y-z), Eq.39 is identical to a conventional finite difference formulation (e.g., Peaceman, 1977; Moridis and Pruess, 1992).

2.4 Closed-Loop Heat Exchange Method

2.4.1 Various Configurations of Closed Loop System (CLS)

There are many reasons that producing fluid directly from liquid-dominated geothermal systems is problematic, whether this is native fluid or a working fluid that is injected and produced for heat recovery, for example:

- (1) the produced fluid may contain dissolved chemical components from the rock making it corrosive to the well and surface collection pipes;
- (2) produced fluid may transport chemical species (e.g., acid gases) from the reservoir to the surface where they must be handled as hazardous pollutants;
- (3) the produced fluid itself may be hazardous and require special handling or incur disposal costs;
- (4) injected working fluid may react with the rock and lead to formation damage, either excessively dissolving the reservoir or plugging it up;
- (5) there may not be sufficient permeability in the geothermal reservoir to inject or recover working fluid at sufficient rates.

One way to avoid these problems is to keep reservoir fluids isolated from the geothermal energy recovery infrastructure through the use of a closed-loop circulation system in which the working fluid never contacts the host rock. For solving it, various configurations of systems exist to isolate the host rock and native geothermal fluids from working fluids for energy recovery. In the first class of designs, the circulation system is installed in a single vertical borehole. For example, ① one such downhole heat exchanger design has U-shaped tubing emplaced in boreholes with perforated casings (e.g., Lund, 2003); ② Another kind of device in a single borehole is the wellbore heat exchanger that includes open-hole sections for limited rock-fluid interaction in low-permeability host rock (e.g., Nalla et al., 2005); ③ Another single wellbore configuration is the coaxial or tube-in-tube design (e.g., Horne, 1980; Wang et al., 2009) with insulated central tubing.

Prior study of single-well closed-loop heat exchange systems using water as working fluid have concluded that the limitations of thermal conduction through the

pipe and into the working fluid, combined with local thermal depletion of the reservoir around the pipe, limit the heat extraction capability of these systems (e.g., Nalla et al., 2005). However, recent developments in reservoir stimulation, drilling technology, and the use of novel working fluids, coupled with the imperative to lower environmental impacts of geothermal energy, are inspiring renewed interest in closed-loop systems.

2.4.2 ECO2G

GreenFire Energy prepared to execute the first demonstration project for **ECO2G™** — “Geothermal Power Generation Using Supercritical CO₂ in a Closed-loop System” (see Figure 8.). **ECO2G** is a dramatically different geothermal power generation technology that will enable thousands of megawatts of new carbon-free power plants in California and other markets. This innovative technology utilizes commercially-proven, off-the-shelf components to produce clean, grid-scale baseload and flexible power at competitive prices without water consumption process. Compared to conventional hydrothermal projects, **ECO2G** uses SCCO₂ instead of water to extract thermal energy through the system. A successful demonstration project is the crucial next step needed to commercialize **ECO2G**.

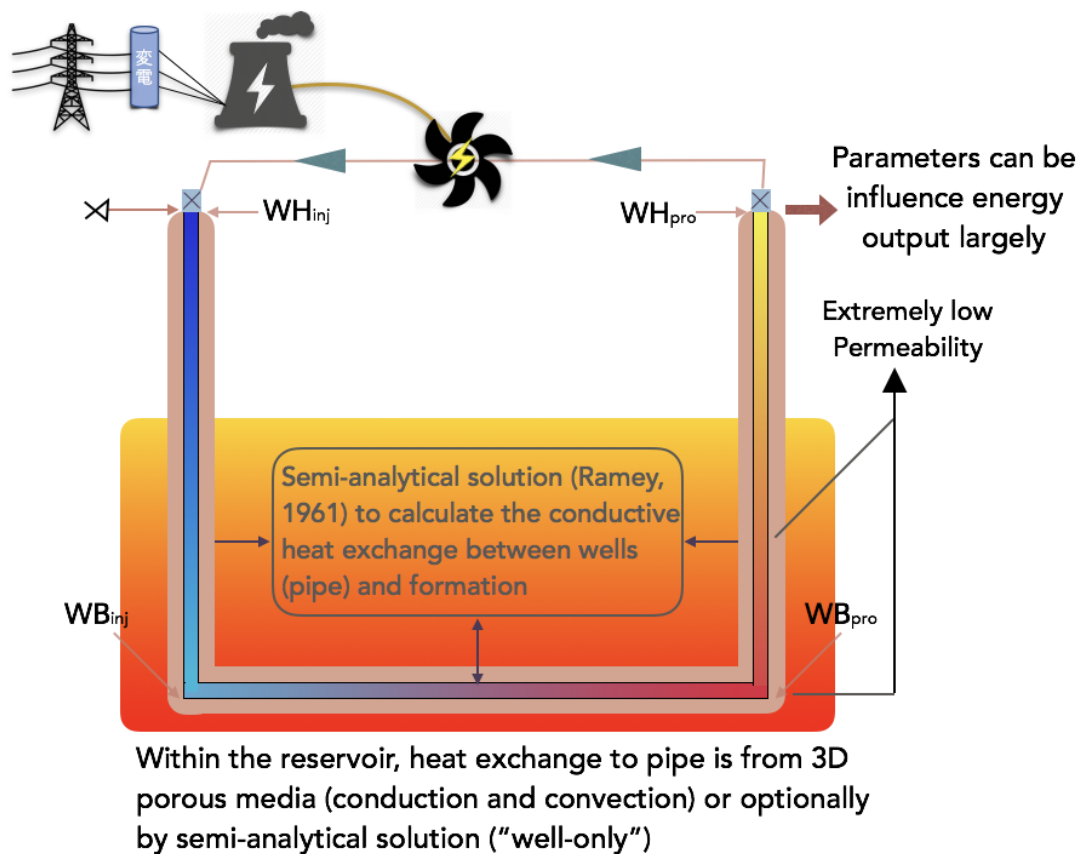


Figure 8. Conceptual Diagram of an ECO2G System

GreenFire has designed, built, and operated an ECO2G demonstration plant using an underperforming hydrothermal well at the Coso KGRA in Inyo County California.

This project would be the first field-scale demonstration of ECO2G technology for geothermal power production. The project is expected to prove that ECO2G can both make utility scale power in large, co-located or greenfield projects or make power from currently unproductive wells. It is anticipated that the project would generate sufficient data to guide the development of commercial projects ranging from 20 MW to 1000 MW.

Although the rare field scale experiment shown at Figure.9 introduced here is not the pattern what we modeled ---- “a wide U-shaped configuration with two vertical sections and a horizontal portion” (see Figure.10), the project involves plugging an existing well above the perforated production liner, and co-axially inserting an insulated pipe to a depth just above the plug. Process fluids, such as supercritical CO₂ will then be injected into the smaller center pipe, and flow downward to the bottom of the well, then return to the surface through the annulus between the two pipes. As the fluid returns to the surface, it will absorb heat and expand, creating the thermosiphon. The fluid then passes through a radial inflow expander/generator set to produce power. To complete the cycle, the process fluid will be cooled before being returning to the well in a closed loop. Along the process pathway, the temperature, pressure, and flow rate of the fluid will be measured.

At this co-axial project, per the plan submitted to the California Energy Commission, would require seven tasks:

- ① General management issues, such as creating reports and permissions.
Preparing the well for the project;
- ② Designing and constructing of ground equipment, including methods for fluid handling as well as actual or simulated power production;
- ③ Preparation for system operations, including system completion and all tests components;
- ④ System operations, including SCCO₂ and water test execution matrices.
- ⑤ Shutdown and site recovery;

⑥ Public relations and technology transfer activities.

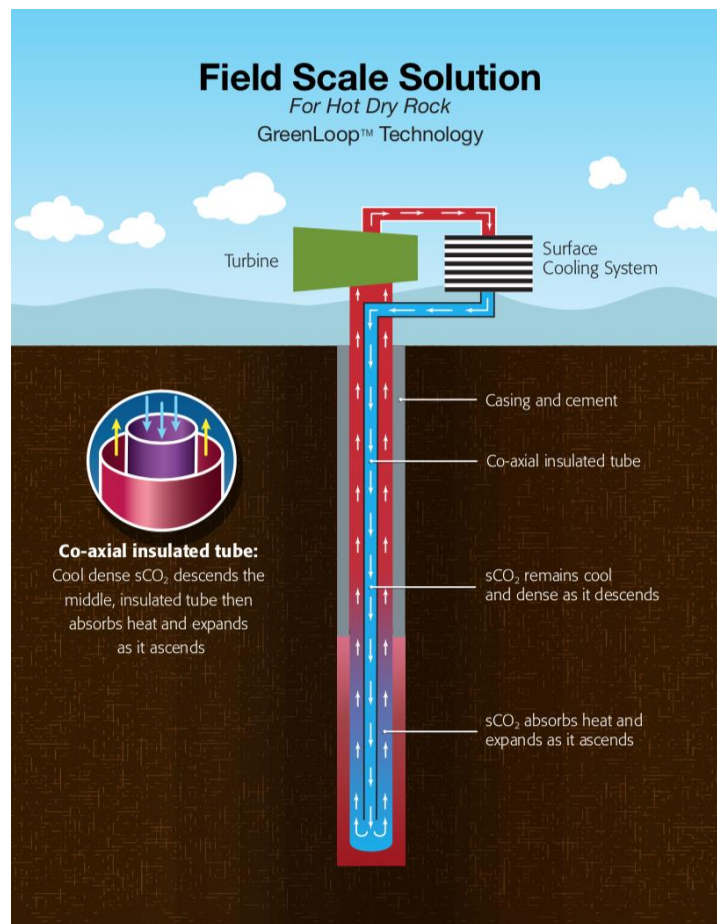


Figure 9. Closed-loop geothermal power system with Co-axial insulated tube provided by GreenLoop™ Technology.

GreenFire's core technology was developed with significant involvement by the US Department of Energy, which has awarded a \$2 million grant to research SSCO₂ power generation in an open system. Extensive early modeling with Lawrence Berkeley National Laboratory (LBNL) indicated that ECO2G can produce commercial scale power without premature depletion of the heat resource. The company then retained Baker Hughes to help build a drilling cost model to determine the economic viability of ECO2G in a wide variety of conditions. More recently, GreenFire and their partners at the Lawrence Livermore National Laboratory were awarded funding under the Department of Energy's Small Business Voucher program. LLNL will perform research

related to novel methods of well completion and directional drilling in hot and deep geothermal formations.

2.4.3 ECO2G versus Conventional Geothermal

There are many existing geothermal fields suffering from reduced production, and the risks and costs of finding and characterizing new areas are hindering investment. Engineering and financial modeling performed by Lawrence Berkeley National Laboratory, **Baker Hughes**, and GreenFire Energy show that developed technology can make a significant contribution to meeting the criteria for renewable portfolios in the competitive California renewable energy market. Substantial recent advances in deep and directional drilling technologies from the oil and gas industry can be applied to extracting geothermal energy from previously inaccessible depths. ECO2G harnesses these technologies to access high-temperature (above 350°C) geothermal resources that cannot be exploited with existing geothermal technology. Many such areas exist in active geothermal regions around the globe.

From written above, ECO2G is very different from conventional hydrothermal projects. The key differentiators are:

- ① ECO2G utilizes SCCO₂ rather than water as the working fluid to carry enthalpy from the resource back to the surface for power production;
- ② The SCCO₂ is circulated through a closed loop well system;
- ③ The ultimate depth of the well system is typically deeper in the geologic formation than the permeable region where water circulates;
- ④ ECO2G's modular architecture and variable-speed turbo expanders allow for both flexible and baseload power generation.

Taken all shown together, the advantages of ECO2G technology overcome the critical barriers that currently limit the ability of conventional geothermal technology to reduce fossil-based energy sources written as follows:

- ① Additional renewable power can be added to the clean energy supply with far less risk, time, and expense than finding and developing new geothermal areas;

- ② ECO2G projects can provide flexible or baseload power on short notice as grid needs and economic returns requirement;
- ③ Existing hydrothermal projects can be useful and made productive for longer periods;
- ④ Existing but unproductive geothermal wells can be rehabilitated and made profitable;
- ⑤ ECO2G provides water-free geothermal power generation when using air-to-air heat rejection.

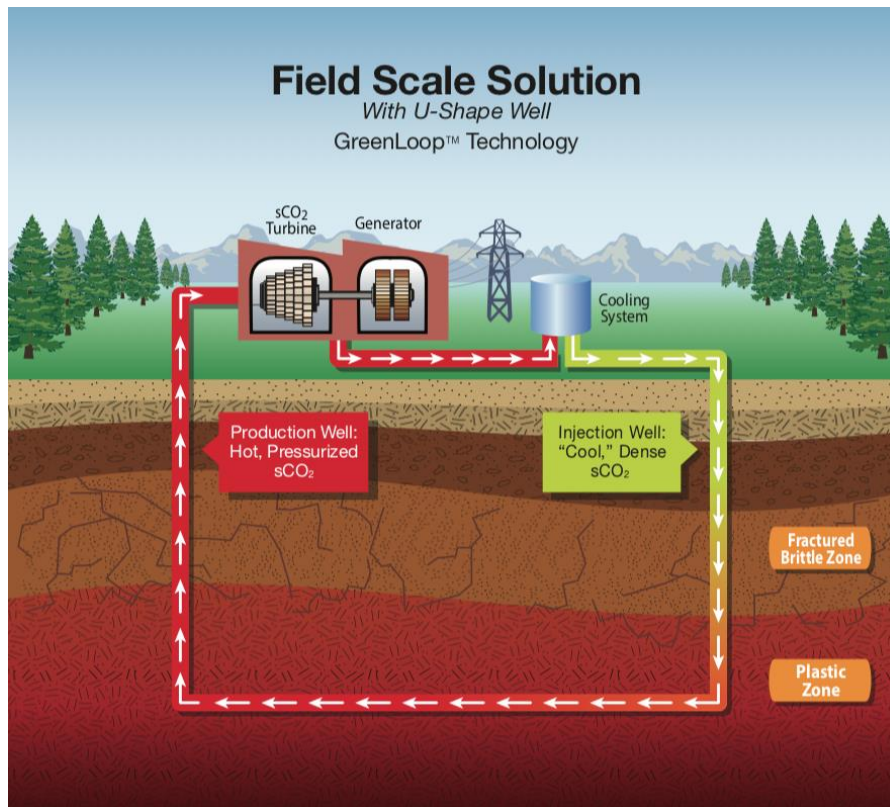


Figure 10. U-shaped configuration geothermal power generation system with two vertical sections and a horizontal portion provided by GreenLoop™ Technology.

2.4.4 Example problems as demonstration for reliability of T2Well

T2Well extends the existing numerical reservoir simulator TOUGH2 by introducing a special wellbore sub-domain in the numerical grid. Wellbore flow is simulated by solving the one-dimensional momentum equation. In the case of two-phase wellbore flow, the Drift Flux Model (Shi et al., 2005; Zuber and Findlay, 1965) combines two momentum equations of two phases to create a single momentum equation of the mixture. As TOUGH2, T2Well also can be used with different EOS to describe different fluid mixtures. Therefore, so far T2Well has been used with ECO2N (Pruess, 2005) for applications related to CO₂ sequestration, with ECO2H (Pan et al., 2011, 2015) for enhanced geothermal system simulations. The heat exchanges between wellbore and the surrounding formation can be numerically simulated, or optionally calculated with Ramey's analytical method (Ramey, 1962) or Zhang's convolution method (Zhang et al., 2011). Details of T2Well characteristics and numerical formulation can be found in Pan and Oldenburg (2013).

The EOS module what we choose to apply at our research is EWASG EOS module, EWASG (Equation-of-state for **W**ater, **S**alt and **G**as) is a TOUGH2 EOS module developed primarily to model hydrothermal systems containing dissolved solids and one non-condensable gas (NCG) such as CO₂, CH₄, H₂S, H₂ or N₂ (Battistelli et al., 1997). EWASG can handle phase equilibria and fluid property calculations up to 350 °C and 100 MPa for H₂O-NaCl-NCG mixtures found in low and high enthalpy geothermal reservoirs, with the limitation of low to moderate NCG partial pressures. However, it is known that EWASG EOS module mainly serves a function in Open-Loop system, what we simulate is Closed-Loop system, where the working fluid never contacts the host rock. In the other word, even the reservoir is governed by H₂O-NaCl-NCG mixtures system, it will be little interaction between H₂O-NaCl-NCG mixtures and closed casing. But, considering the heat conduction, advection and convection at different EOS controlled reservoir have different effect, we still adopted EWASG EOS module in geothermal power generation system.

Here, in order to inspect and verify the reliability of T2Well, there are 3 example problems which simulated by T2Well and some general questions are demonstrated so

that the reliability of T2Well is checked to some extent.

First, it did the validation of wellbore flow in geothermal wells, using the example called “Steady-state two-phase flow upward (comparison against analytical solutions)”. To verify the wellbore flow solution approach, LBNL simulated a case (Case 1) of steady-state, isothermal, two-phase (CO₂ as gas and water as liquid) flow through a vertical wellbore of 1000 m length. The details of the problem are described below (Table 2):

Table 2. Parameters of the two-phase wellbore flow problem

Parameter	Value	Note
Length	1000 m	Vertical wellbore
Diameter	0.1 m	Circular
Total (upward) mass flux (G)	50 kg/m ² /s	Gas + Liquid
Gas mass fraction	0.5	$S_G \rho_G u_G / G$
Temperature	40 °C	Isothermal
Wellhead Pressure	10 ⁵ Pa	

The specifications of the one-dimensional numerical solution (T2Well/ECO2N) are:

1.	1000 m wellbore with a diameter of 0.1 m
2.	Grid resolution 10 m
3.	Injection mass rate at bottom: CO ₂ : 0.19625 kg/s; water: 0.19625 kg/s (Each = 25 kg/m ² /s with a cross sectional area of 7.8500E-03 m ²)
4.	Isothermal simulation with a uniform temperature of 40°C throughout the well
5.	Top boundary (outlet) pressure is 10 ⁵ Pa
6.	Wall roughness 2.4e-5 m

The steady state problem is actually solved as a transient problem with adaptive time steps. The ending simulation time is 0.456869E+09 seconds (4100 steps), at which the average pressure loss due to temporal acceleration is about 3.80E-16 (Pa/m). Therefore, the steady state is considered can be reached.

As shown in Figure 11, the numerical solutions are almost identical to the analytical solutions (Pan et al., 2010), thereby verifying the numerical wellbore code (T2Well/EOS3) for this particular problem. Note that the mixing between the CO₂ and the water phases is allowed in the numerical simulation but no mixing is assumed for the analytical solution. However, the almost perfect match between analytical solutions and the numerical solutions implies that the effects of the mixing between the two phases (<2%) on the two phase flow are negligible.

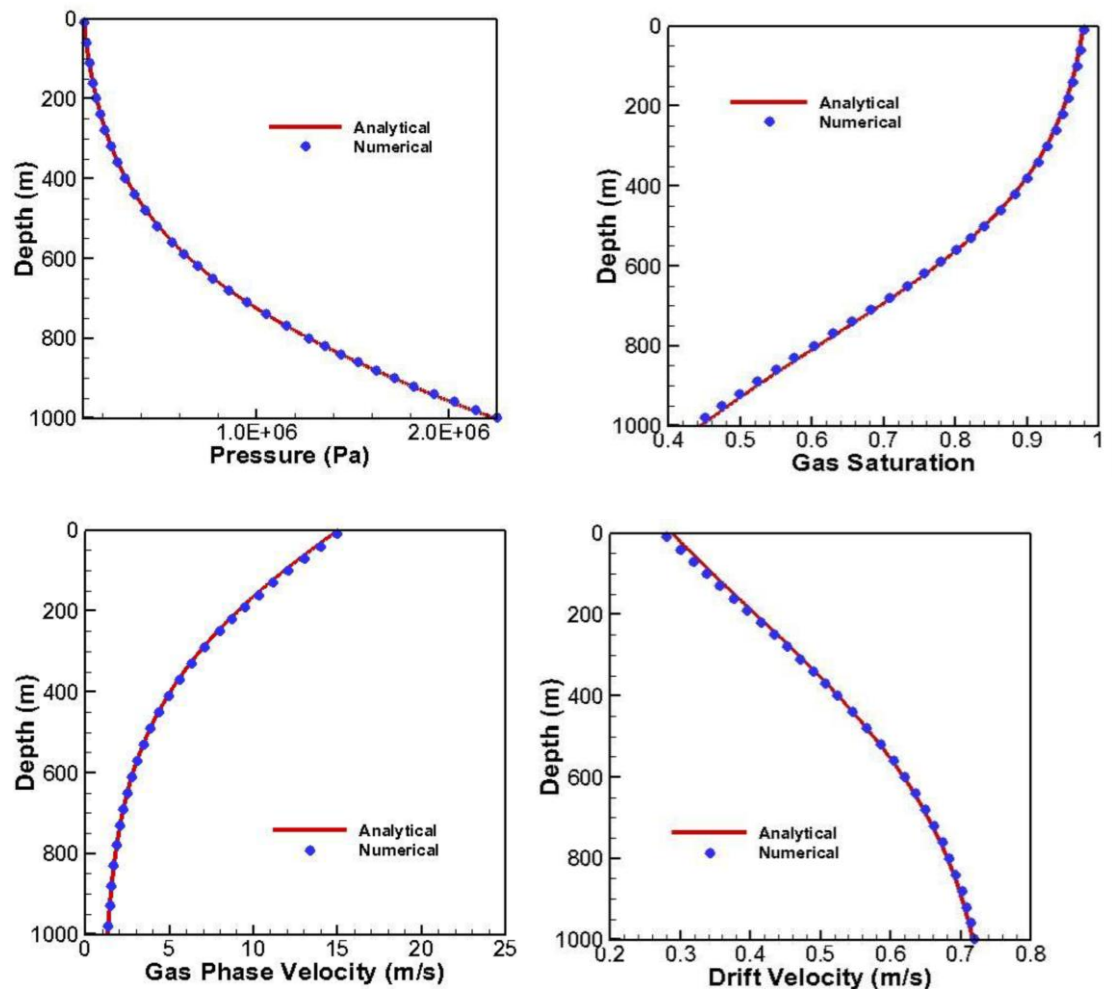


Figure 11. Case 1: Distribution of pressure, gas saturation, gas-phase velocity, and drift velocity under steady-state, isothermal, two-phase (CO₂/water) flow conditions in a vertical wellbore showing excellent agreement between the two approaches.

In this system, although the mass fraction (CO₂ : H₂O) is constant (X =0.5) throughout the wellbore, the gas (CO₂-rich phase) saturation decreases with depth due to pressure increase because of the low density of gas phase at the given pressure range (Figure 11). Meanwhile, the drift velocity (of the gas phase relative to the mean volumetric velocity) increases with depth from about 0.28 m/s to 0.72 m/s. However, the gas-phase velocity decreases with depth by about 11 times over 1000 meters. The results of Case 1 show us T2Well can work well and accurately in vertical wellbore part.

Next, the Case 2 titled “Non-isothermal CO₂ flow through a wellbore initially full of water” was be simulated. This problem is a case of two-phase flow up an open well bore. The scenario envisioned is the tip of a migrating CO₂ plume at 10% gas saturation encountering an open well initially filled with water. what focus here is on flow in the wellbore. The reservoir is assumed to be able to maintain the constant pressure, temperature, and gas saturation during the process. Starting from hydrostatic conditions and a geothermal temperature gradient in the well, an overpressure of 0.1 MPa (1 bar) is applied to the reservoir to mimic an injection-induced overpressure. Wellbore heat transmission to the formation is calculated with the analytical solution. Figure 12 shows part of the input file for Case 2 (with brine in reservoir).

```

*Leakage wellbore DFM* ... 1-D column to 1000 m depth, 10 m vertical grid spacing,0.1 dia
ROCKS---1---*---2---*---3---*---4---*---5---*---6---*---7---*---8
wellb 2 2600.e00 1.0000 200.0e-9 200.0e-9 200.0e-9 -2.51 920.
0.0e-10
7 .457 .05 1. .05
8
wtmos 2 2600.e3 1.0000 200.0e-9 200.0e-9 200.0e-9 2.51 920.e-3
0.0e-10
7 .457 .05 1. .05
8
botwe 2 2600.e00 0.5000 2.0e-12 2.0e-12 2.0e-12 2.51 920.
0.0e-10
7 .457 .01 1. .01
8

MULTI---1---*---2---*---3---*---4---*---5---*---6---*---7---*---8
3 4 3 6
SELEC...2...3...4...5...6...7...8...9...10...11...12...13...14...15...16
1 0 0 0 0 0 0 0 0
.8 .1 1.2 1.53 0.1 0.046e-3

```

```

SOLVR---1---*---2---*---3---*---4---*---5---*---6---*---7---*---8
5 ZI O0 8.0e-1 1.0e-7
START---1---*---2---*---3---*---4---*---5---*---6---*---7---*---8
---*---1 MOP: 123456789*123456789*1234 ---*---5---*---6---*---7---*---8
PARAM---1---*---2---*---3---*---4---*---5---*---6---*---7---*---8
28100 1001000300000200 4 3
3.6e+4 2.e-1 2.0e+1 9.81 2.0
1.E-4 1.E00
1.013e5 0.0 1.0 15.
GENER---1---*---2---*---3---*---4---*---5---*---6---*---7---*---8

... ..

ELEME ---
*ta 1 wtmos1.0000E+50 4.0991E-024.0320E-02 1002.000
1Aa 1 wellb7.8500E-020.0000E+00 4.0991E-024.0320E-02 997.000
1Ba 1 wellb7.8500E-020.0000E+00 4.0991E-024.0320E-02 987.000
1Ca 1 wellb7.8500E-020.0000E+00 4.0991E-024.0320E-02 977.000

... ..

INCON -- INITIAL CONDITIONS FOR 102 ELEMENTS AT TIME 0.256091E+11

... ..

*ta 1 0.90000000E+00
0.1013253378869E+06 0.000000000000E-04 1.000000000000E+00 0.350000000000E+02
bba 1 0.50000000E+00
0.9983837982470E+07 1.200000000000E-01 1.010000000000E+01 0.650000000000E+02

ENDCY---1---*---2---*---3---*---4---*---5---*---6---*---7---*---8

```

Figure 12. Input file (portion) of Case 2. Note X2 (mass fraction of NaCl in liquid phase) = 0.12 for the reservoir cell “bba 1”, indicating the brine aquifer. For no salt case, this X2 = 0.0.

In Figure 13., it shows gas saturation, gas density, pressure, and temperature throughout the well as a function of time. As shown, the well is initially filled with water and gas enters progressively from the bottom up. After 10 minutes (600 s), gas is fairly evenly distributed throughout the well from 10% at the bottom to nearly all gas at the top. The reason for this increase in gas saturation is the exsolution of gas from the liquid as pressure drops and the large expansion that CO₂ undergoes as it transitions from supercritical to gaseous conditions. This transition occurs around the critical pressure (7.4 MPa) at a depth of approximately 755 m. The gas density plot shows the sharp decrease in gas density in that region. Temperature also affects CO₂ solubility, but temperature becomes relatively constant as the steady flow develops resulting in

decreasing CO₂ mass fractions being controlled mostly by pressure. The temperature contour shows the evolution from a conductive profile controlled by the geothermal gradient to an advective profile controlled by upward fluid flow. In between the initial and steady states, there are some local maxima arising from the expansion of CO₂ as gas phase rises upwards and transitions to gaseous conditions.

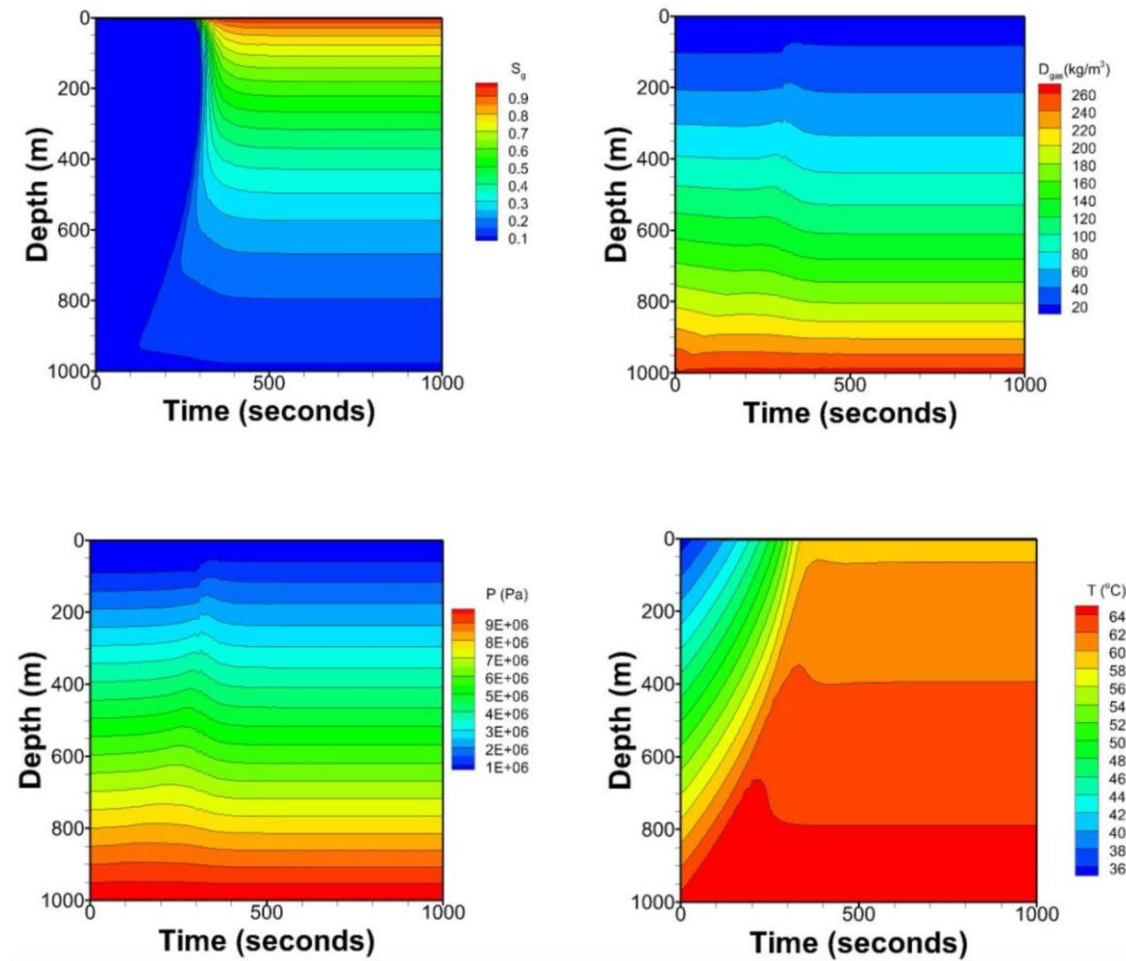


Figure 13. Case 2: Profiles of gas saturation, gas density, pressure, and temperature in the wellbore as a function of time.

Figure 14 shows the CO₂ leakage rates at wellhead from a no-salt aquifer and a brine aquifer under the same conditions. The final flow rate is reduced from 2.33 kg/s of no-salt case to 1.63 kg/s of brine case with slightly delay in the breakthrough of CO₂ too. This is simply because, in this two phase flow situation, heavier brine means more

hydrostatic pressure loss so that there is less energy could be used to move CO₂ upward in the brine case than in the no-salt case, for the same injection-induced overpressure.

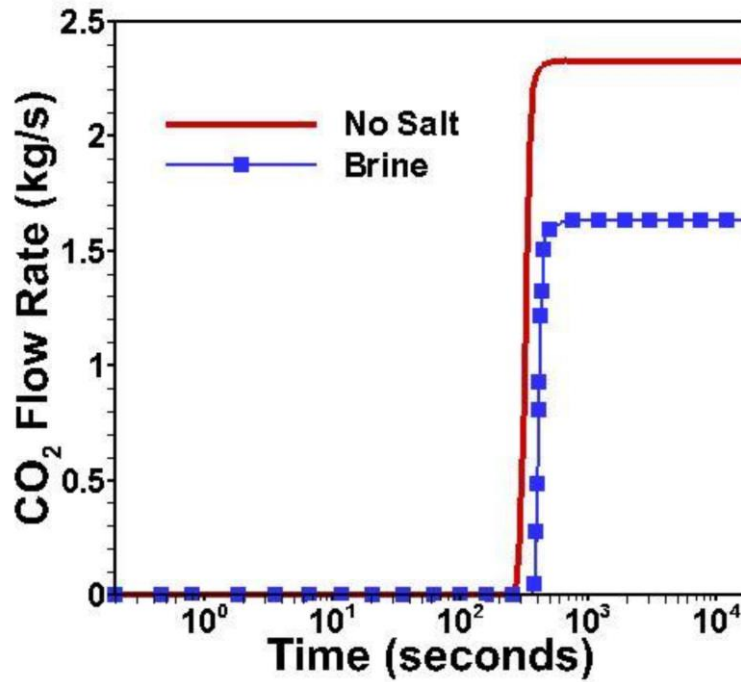


Figure 14. Case 2: The effect of brine on CO₂ leakage rate through wellhead.

Mass fraction of salt in the brine is 0.12. All other conditions are the same.

Last, the Case 3 titled as “Injection of CO₂ into a depleted gas field”. The problem is a case of injection of CO₂ into a depleted gas field through a wellbore at a depth of 3000m below surface. The focus here is to investigate if the lower pressure in the reservoir could cause a “choke” in wellbore flow due to the down-hole transition to subcritical (gaseous) conditions. The reservoir is assumed to have a thickness of 100m and an area of 1 km by 1 km. It is fully perforated by a wellbore of 0.18m in diameter. The initial pore pressure in the reservoir is ≤ 3.4 MPa. The initial temperature in the reservoir is 90°C whereas the temperature in the wellbore gradually reduces to 35°C as it approaches the surface. An impermeable layer with a constant temperature of 90°C is under the reservoir. The formation permeability of the reservoir is 10^{-13} m^2 .

The injection rate is 100 kg/s at a temperature of 60°C. A 2D radially symmetry grid with 416 cells (31 well cells) is used.

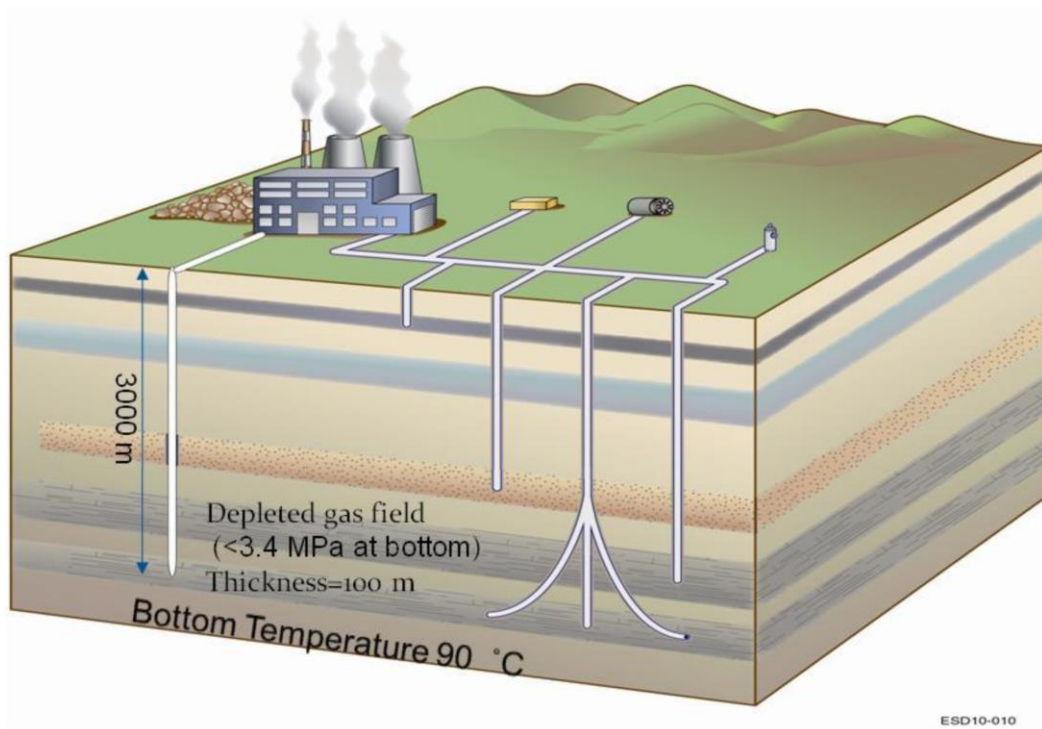


Figure 15. Sketch of injection into a depleted gas field.

As shown in Figure 16, the lower pressure in the wellbore quickly disappears with the injection of CO₂. Within one day of injection, most of the wellbore reaches the supercritical condition (Figure 16c) and the entire wellbore is in the supercritical condition after about 240 days of injection (Figure 16a). Meanwhile, the temperature profile also quickly transforms from a geothermal gradient dominated one into a convection dominated one within 1 day (Figure 16d) and then becomes relatively uniform (Figure 16b).

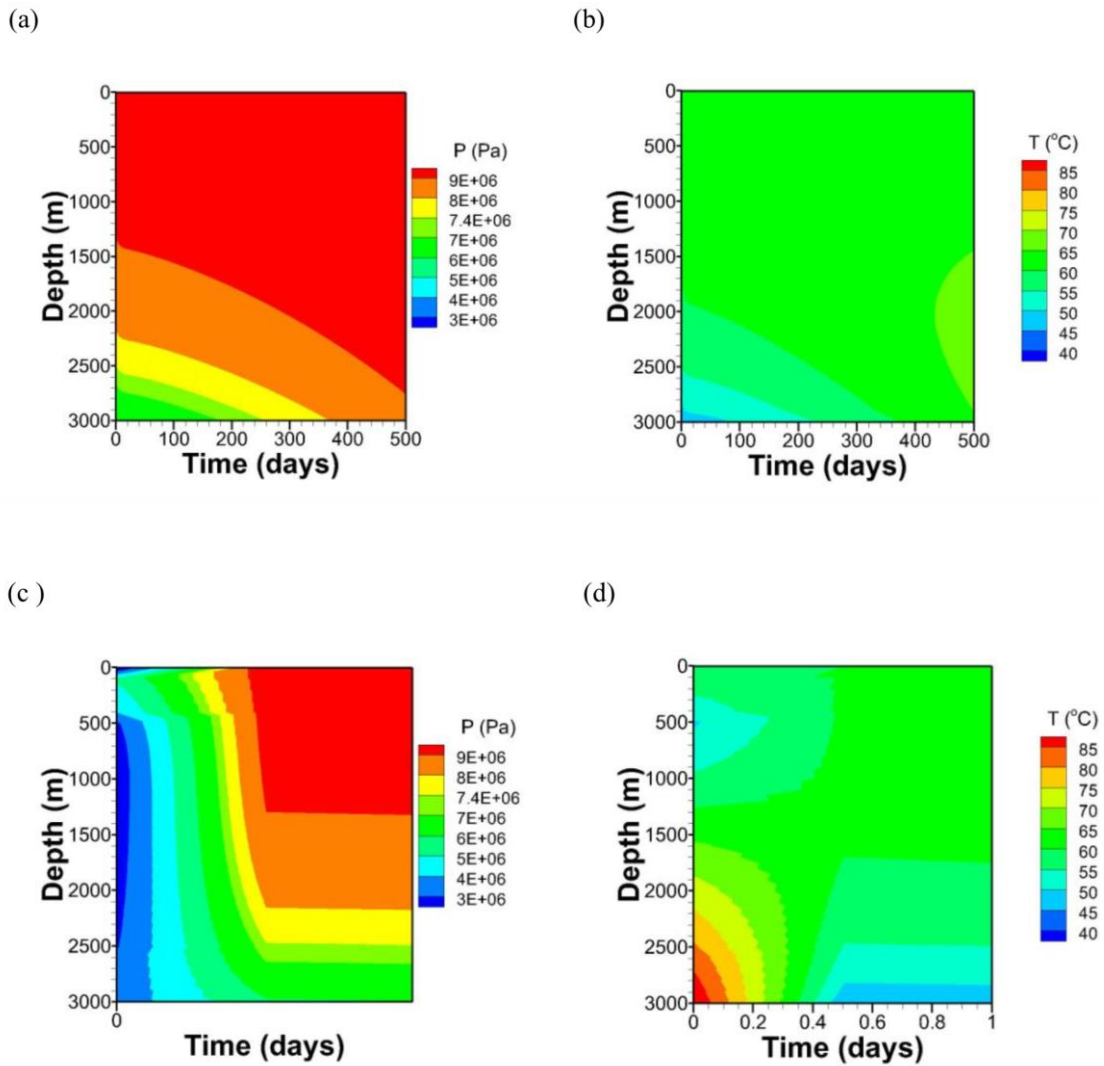


Figure 16. Case 3: Profiles of pressure and temperature in the injection wellbore as a function of time. (c) and (d) are short time (the 1st day) plots of (a) and (b).

The wellhead pressure quickly (within 1 day) reach above 9 MPa and stay there until the front hits the lateral boundary of the reservoir so that the pressure in the entire reservoir rises to above the critical pressure (Figure 17). Although the low-pressure at reservoir does keep the lower portion of the wellbore under subcritical condition for a significant period, it does not cause a persistent “choke” in the vertical wellbore. In other words, an extremely high wellhead pressure is not needed to maintain the given injection rate.

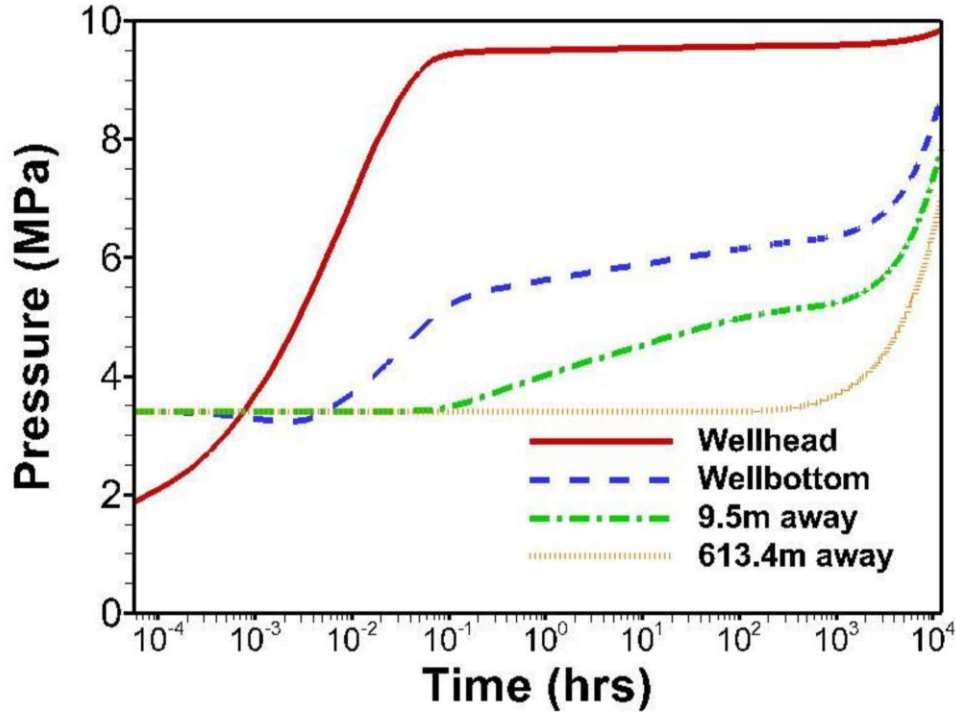


Figure 17. Case 3: Pressure responses to the injection at wellhead, well bottom, and two locations in the reservoir.

By the introduction of these three typical example cases, it indicates the T2Well can be used in many kinds of systems with a relatively high reliability and precision. Currently, because there is extremely few field-scale experiment of EGS geothermal power generation system and ECO2G system, the simulation method become a main research means to do the new concept geothermal projects.

Therefore, here we decided to use T2Well developed by **LBNL** as research tool to simulate a Closed-Loop geothermal power generation system using SCCO₂ as working fluid referring the ECO2GTM Technology promoted by **GreenFire Energy**.

Chapter 3 : Model Information

3.1 Introduction for Construction of model

Consider observing how a typical Closed-Loop geothermal power generation system works, here we adopted a relatively ideal geological information model from Imperial Valley with a regular thermal gradient and without fault that was applied in Curtis M. Oldenburg, Lehua Pan and Mark P. Muir (2016). The reservoir is assumed to be a liquid-dominated geothermal reservoir in permeable sediments at a depth of approximately 2500m with hydrostatic pressure of 25MPa and initial temperature of 250°C. The discretized domain and the vertical sections of the well (red lines) are shown in Figure 18a.

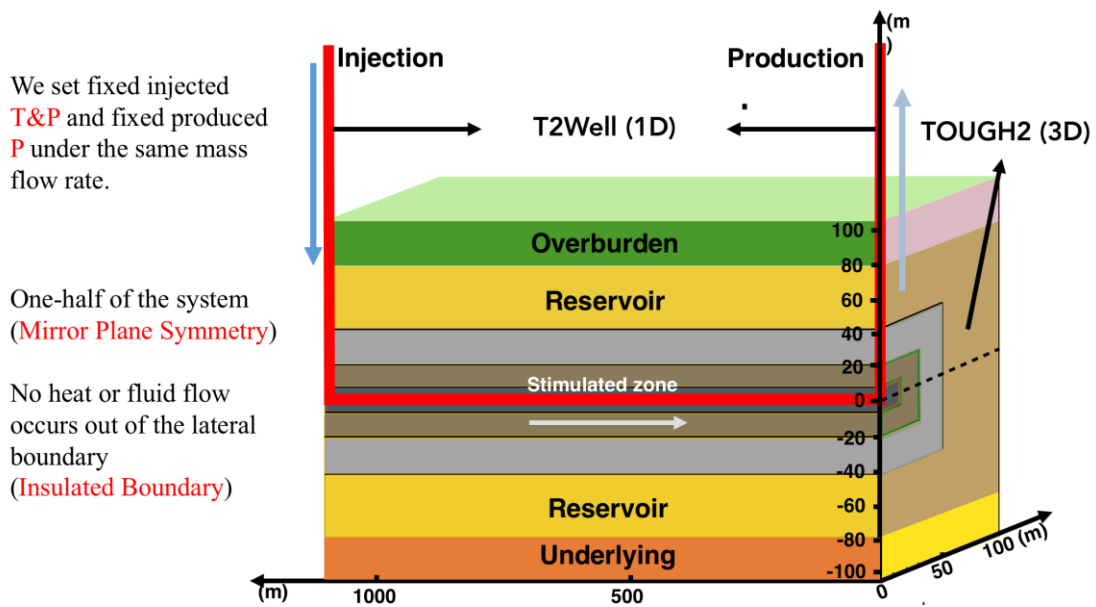


Figure 18: Discretization of the reservoir part of the closed-loop model 3D domain (blue = overburden, red = underburden, green = reservoir region) including the vertical legs (red lines) of the closed-loop well.

GreenFire Energy’s GreenLoop changes all of this by using a variety of refrigerants (H₂O, CO₂) that have been optimized to circulate in a sealed, closed-loop system that penetrates geothermal regions. Creating a closed-loop system requires many of the same advanced drilling and completion technologies that revolutionized the oil and gas

industry. A closed-loop system has the twin benefits of preventing the loss of refrigerant, and of keeping the refrigerant stream from interacting with water and minerals that would otherwise result in scaling and corrosion.

As shown above, we model one-half of the system due to mirror plane symmetry characteristic along the axial direction of the horizontal section of the well and assume no heat or fluid flow occurs out of the lateral boundary, such as might be appropriate if there were a series of these U-shaped wells installed parallel to each other 100 m apart in the reservoir.

In Figure 19a, it shows a vertical cross section through the horizontal section of the well showing the graded discretization with refinement around the well. Note the 40 m x 40 m region around the well that will be modeled as a stimulated region. The details of the refinement around the well are shown in Figure 19b.

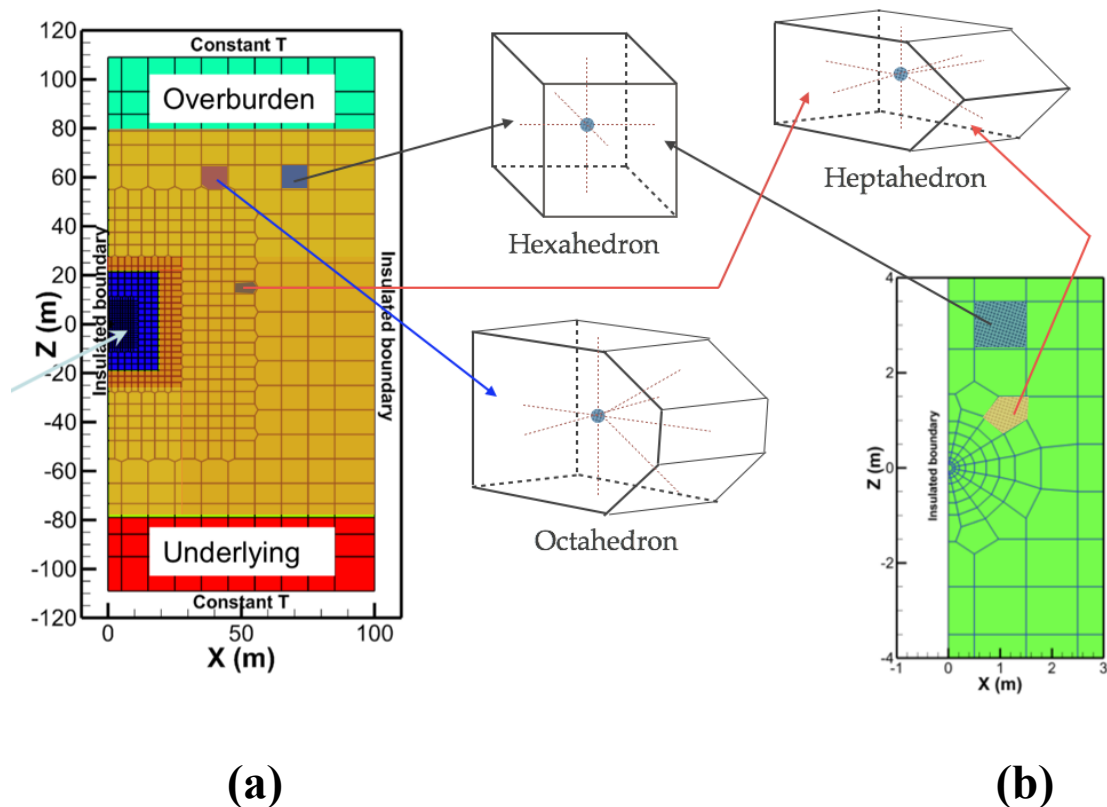


Figure 19. Discretization of the reservoir part of the closed-loop model showing (a) cross section of the horizontal well region; (b) closeup of the well region.

We have carried out mixed convective-conductive fluid-flow modeling using a wellbore flow model for TOUGH2 called T2Well to investigate the critical factors that control closed-loop geothermal energy recovery. T2Well solves a mixed explicit-implicit set of momentum equations for flow in the pipe with full coupling to the implicit three-dimensional integral finite difference equations for Darcy flow in the porous medium. T2Well has the option of modeling conductive heat flow from the porous medium to the pipe by means of a semi-analytical solution, which makes the computation very efficient because the porous medium does not have to be discretized. Here, the fully three-dimensional option is chosen, thus the porous medium is discretized and heat flow to the pipe is by conduction and convection, depending on reservoir permeability and other factors. Simulations of the closed-loop system for a variety of parameter values have been carried out to explain the heat recovery process. To the extent that convection may occur to aid in heat delivery to the pipe, the permeability of the geothermal reservoir, no matter what natural or stimulated, is an important property in heat extraction.

Besides reservoir, wellbore is also a very important factor in all system. In this closed-loop system, unlike conventional EGS consisted by vertical wellbores only, there is horizontal wellbore existed in the system. In fact, in our closed-loop system, there is a U-shaped well consists of a long (1 km) horizontal wellbore within the reservoir connected to two 2.5 km-long vertical injection and production sections. Base-case properties of the well and CO₂-injection and production conditions are shown in Table 3. The total length of the wellbore is 6.1 km. The working fluid (CO₂) is introduced at the inlet side (left-hand side in Figure 18) and produced out of the outlet on the right-hand side. Thermal conductivity of steel is 50.2 W/ (m K), much higher than that of the reservoir rock and can therefore be ignored in the model.

Table 3. Properties of the wellbore.

	Horizontal Wellbore	Vertical Wellbores
Parameter	value	
Length	1100m	2500m (lateral)
Diameter	0.168m	0.168m
Material	steel	steel
Tube	0.154m	0.154m
Roughness	4.57e-5	4.57e-5

3.2 Preparation of Input Data

3.2.1 Initial Condition

The properties of various specific regions in the closed-loop model is relatively different, and even a little change in one region will affect the overall energy gain very much. As shown in Table 4., 4 main governing regions have been set by thickness, porosity and so on. Especially, We pointed out the set of simulations presented here assume a reservoir under liquid-saturated conditions whose thermal conductivity is 4 W/(m °C), consistent with measurements of sandstone (e.g., Zimmerman, 1989).

Table 4. Properties of various regions in the closed-loop reservoir model.

Zone	Overburden	Reservoir	Underlying	High-k zone around well
Thickness (m)	155	158	55	40
Porosity (vol%)	5	25.4	5	25.4
Rock grain Density (kg m ⁻³)	2700	2700	2700	2700
Rock grain specific heat (J/(kg°C))	1000	1000	1000	1000
Thermal conduction (W/(m°C))	4.0	4.0	4.0	4.0
Pore Compression (Pa ⁻¹)	7.25×10^{-12}	7.25×10^{-12}	7.25×10^{-12}	7.25×10^{-12}
K (m ²)	10^{-15}	10^{-12}	10^{-15}	10^{-10}

In T2Well of the closed-loop geothermal system, there are 4 main governing regions — “Overburden, Underlying, Reservoir, Stimulated zone”. The spatial relationship is seen at Figure 18., and how many elements in each region respectively will be written at Table 5.

Table 5. The numbers and volume range of reservoir system.

	Elements	Volume range (m³)
Overburden	520	3380 ~ 500000
Reservoir	4836	312 ~ 15000
Stimulated Zone	4916	0.118 ~ 625
Underlying	520	3380 ~ 500000

There are 10792 reservoir elements as surrounding formation and 67 wellbore elements for working fluid circulating to extract heat from ground. Therefore, the closed-loop geothermal system model consists of totally 10859 elements. The specific volume for elements of different regions are shown at Table 6 as follows:

Table 6_1. The numbers and volume of reservoir domain.

Volume(m³)	312	313	469	625	938	1020	1210	1250	1410
Elements	13	26	26	767	211	260	26	78	26
Volume(m³)	1880	2420	2460	2500	2880	3750	4060	4130	4840
Elements	26	221	52	1235	26	221	260	26	26
Volume(m³)	5630	5750	8250	8630	9690	9840	10000	12400	15000
Elements	26	208	208	26	221	52	364	26	169

Table 6_2. The numbers and volume of overburden or underlying domain.

Volume(m³)	3380	4620	6750	7000	9250	10100
Elements	13	13	104	13	104	13
Volume(m³)	13900	14000	21000	100000	150000	500000
Elements	13	104	13	104	13	13

Table6_3. The numbers and volume of stimulated zone domain.

Vol.(m ³)	Elem.						
0.118	39	11.600	13	37.585	13	100.000	2119
0.235	91	11.700	13	42.300	13	175.000	65
0.268	26	12.000	13	42.548	13	180.000	208
0.536	91	12.103	13	42.700	39	192.000	208
0.629	26	12.660	13	42.937	13	301.000	26
0.940	2	13.200	13	50.000	182	306.000	26
1.260	91	13.300	13	66.296	13	313.000	65
1.450	26	13.759	13	87.500	26	603.000	65
2.830	26	30.764	13	92.300	13	604.000	104
2.900	91	31.686	13	92.700	13	614.000	52
5.650	91	34.605	13	94.960	13	625.000	767
8.540	91	36.913	13	96.342	13		

After setting for reservoir formation model, regardless of whether extra compression is needed or not, as CO₂ flows down the well into hot regions of the subsurface, its energy changes as it loses gravitational potential, heats up by compression and by absorbing heat through the hot pipe wall, and as its velocity changes. These four forms of energy, pressure-volume, thermal, kinetic, and gravitational potential are all accounted for in T2Well in the output energy gain (MW) that we will calculate and report below. We observe that because mass is conserved in the pipe, and the inlet is at the same elevation as the outlet, the gravitational potential energy difference across the system is always zero.

We set 3 cases to observe how injection mass flow rate will affect overall energy gain (MW), and each case set three sub-case to observe how injection temperature will affect overall energy gain (MW). Meanwhile, whether thermosiphon will give a positive effect to energy gain and cost saving for pump or not. Case input information written at Table 7 as follows:

Table 7. Input information for 3 cases.

	Mass flow rate (kg/s)	T_{inj} (°C)	P_{inj} (MPa)	P_{out} (MPa)
Case 1_1	40	30	7	6.9
Case 1_2	40	40	7	6.9
Case 1_3	40	50	7	6.9
Case 2_1	60	30	7	6.9
Case 2_2	60	40	7	6.9
Case 2_3	60	50	7	6.9
Case 3_1	80	30	7	6.9
Case 3_2	80	40	7	6.9
Case 3_3	80	50	7	6.9

3.2.2 Boundary Condition

we model one-half of the system (mirror plane symmetry) along the axial direction of the horizontal section of the well and assume no heat or fluid flow occurs out of the lateral boundary. Besides, the model system has a constant-temperature boundary condition at the bottom and top that serves to replenish heat.

The diagram of closed-loop geothermal system model with boundary is shown in Figure 20 as follows:

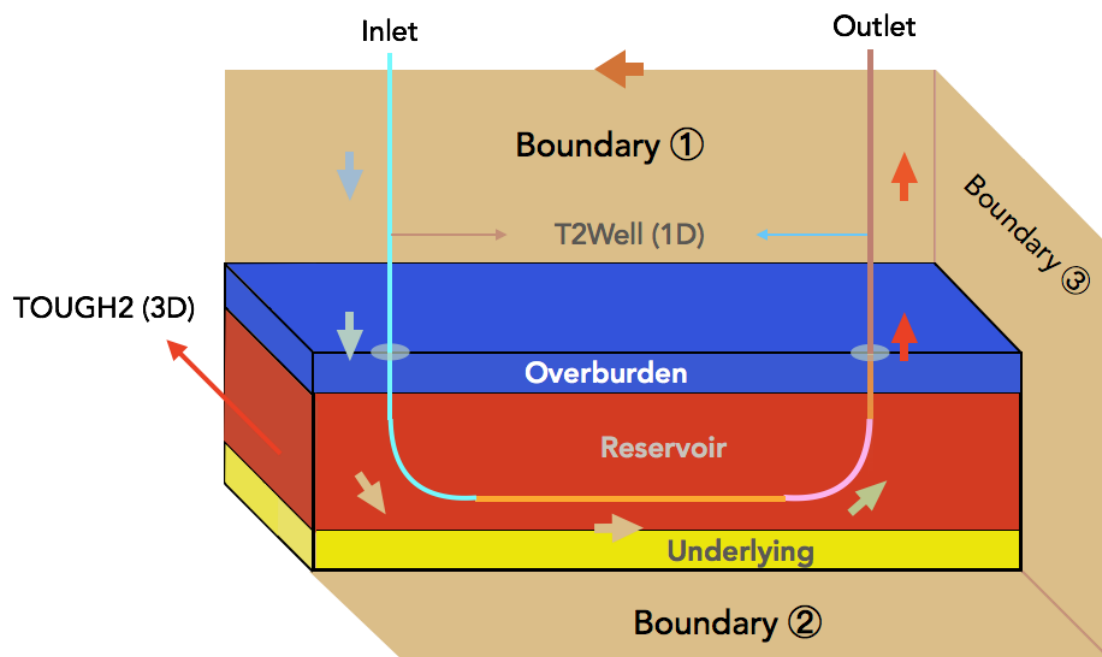
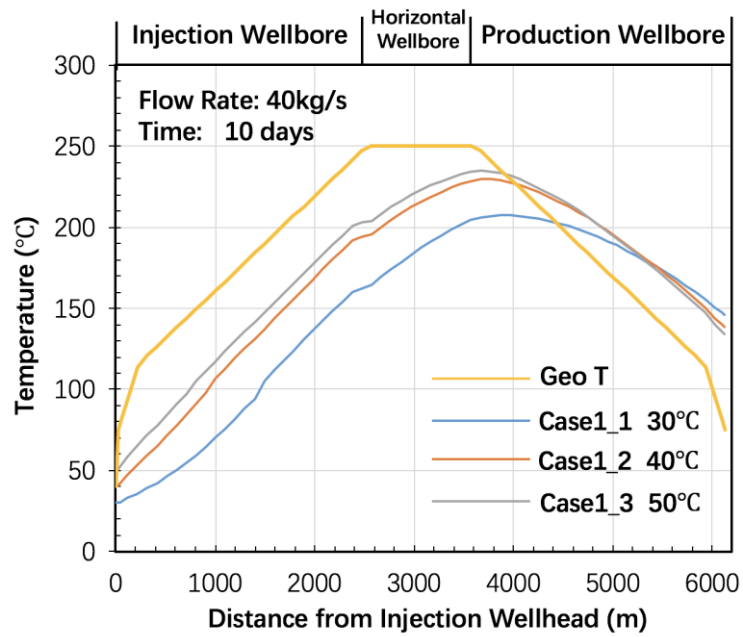


Figure 20. Diagram of the closed-loop geothermal system model with boundary.

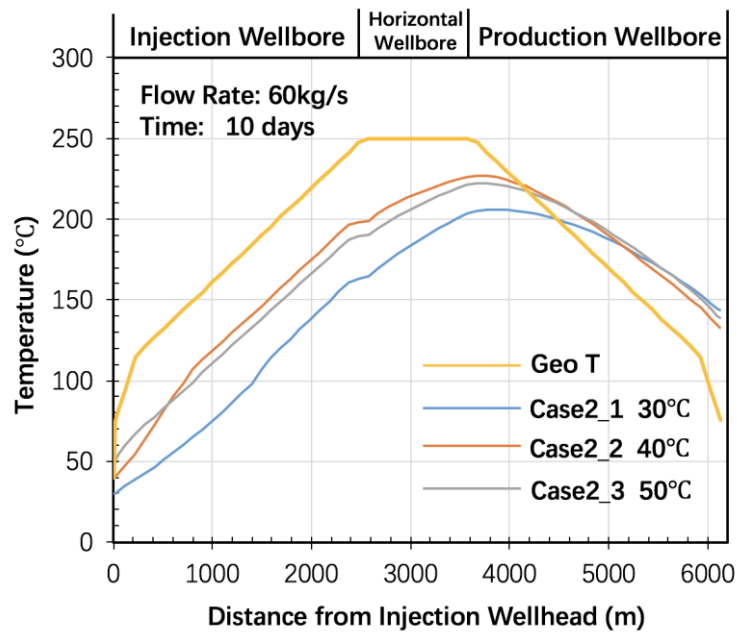
Chapter 4 : Results and Analysis

4.1 Temperature

We mainly simulated 10-day operation of closed-loop geothermal power generation system for all 9 subcases. First, results of temperature profile through the pipe-reservoir system for Cases 1, 2, and 3 for the full-reservoir (3D) system are shown in Figure 21.



(a)



(b)

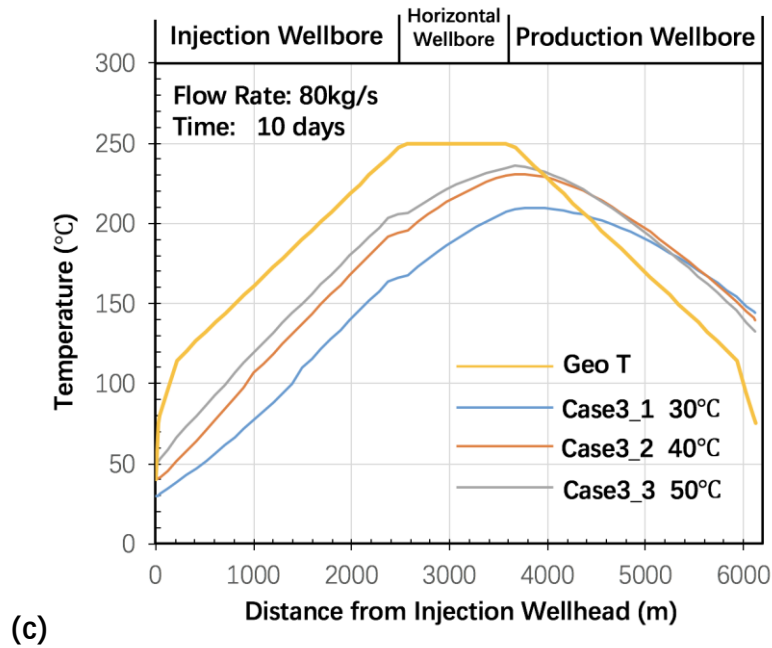


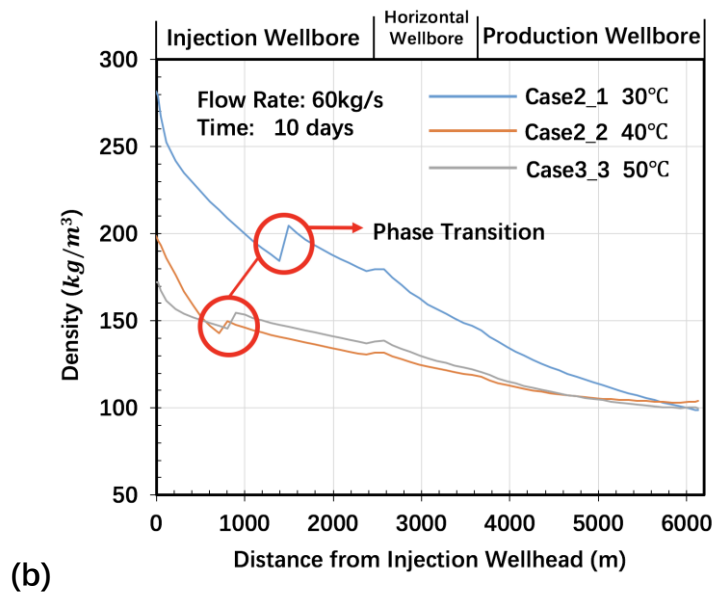
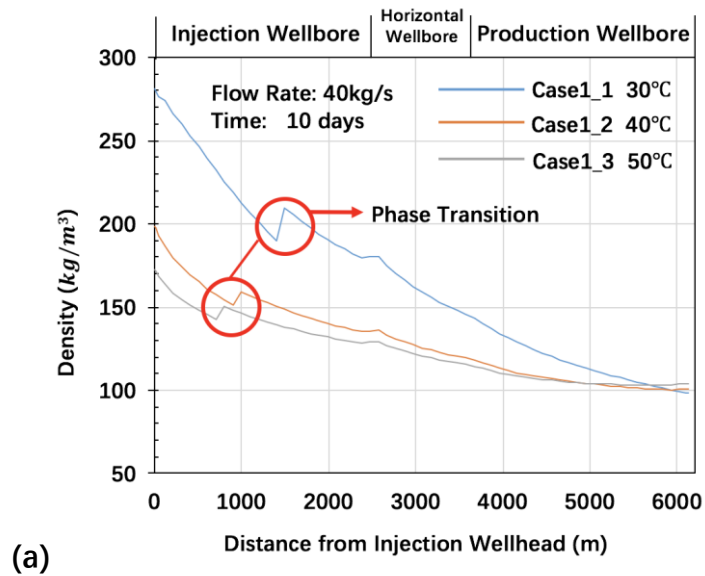
Figure 21. Temperature profile within 10 days with different injection conditions.

As to Case 1 and Case 2, the low mass flow rate (40kg/s) and middle mass flow rate (60kg/s) produce about 1.27~2.11 MW and 2.01~3.11 MW respectively at nearly steady state. Under setting condition, no matter how mass flow rate changes, the low injection temperature always reach the high temperature at outlet, and the highest injection temperature (50°C) subcase always reach the lowest output temperature,

We note also in Figure 21(a)(b)(c) that CaseX_1 starts from 30°C, as the lowest injection temperature, CaseX_1 always can reach the highest output temperature among the same flow rate Case. Along injection wellbore, the Cases of the same flow rate and different injection temperature almost keep the similar increasing rate. However, the decreasing rates along production wellbore become different, compared to CaseX_2 and CaseX_3, CaseX_1 has a lower temperature decreasing rate. The reason why only CaseX_1 can decrease slower than other cases is related to density profile and the state of CO₂ at inlet.

4.2 Density and Phase Transition

We found there exists a few relationship between temperature and density profile diagrams. When the fierce density change occurs at someone depth along injection wellbore, there must be a corresponding wave motion occurs in temperature profile (see Figure 22).



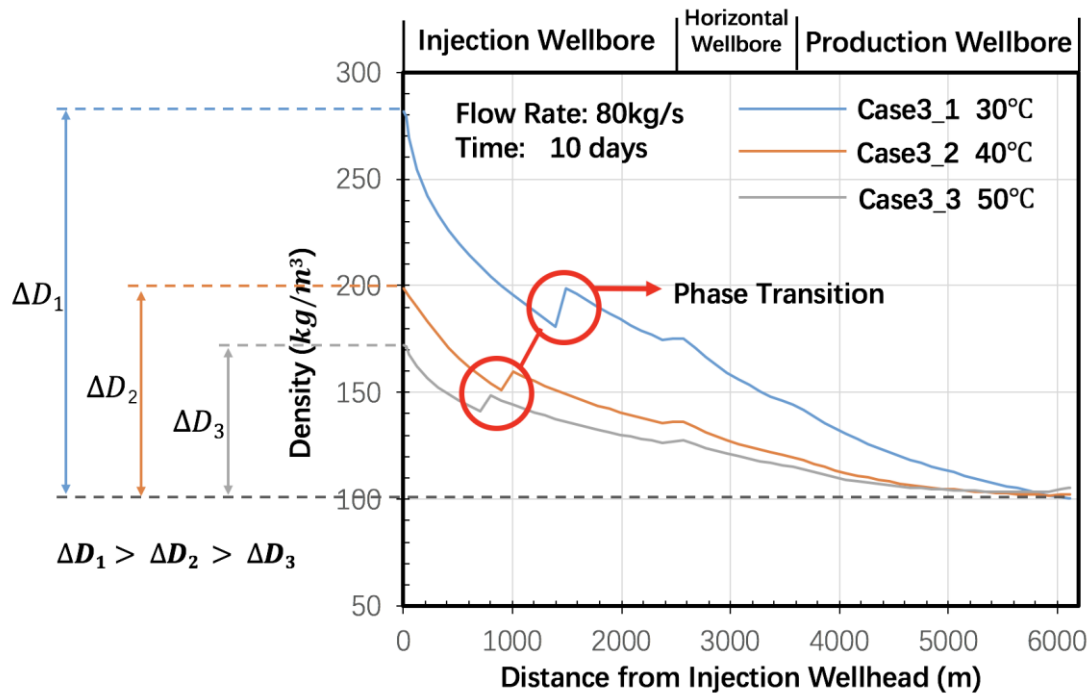


Figure 22. Simulation results of the effect of different CO₂ injection temperature on density change in closed loop under different mass flow rate.

Mass flow rate: (1) 40kg/s; (2)60kg/s; (3)80kg/s.

All 9 subcases have the quick density change along injection wellbore, it indicates working fluid CO₂ has a phase change from subcritical to supercritical state and some marked change occur on the term of density. Even it's said that liquid CO₂ and supercritical CO₂ have the similar density property, but there still exists an obvious difference on density between these two phase. And the property of subcritical CO₂ is close to gas, thus there is sufficient evidence to speculate that the fierce density change caused by phase transition from subcritical to supercritical completely. Take Case3_1 as an example, the temperature (heat) circulation cycle as shown in Figure 23.

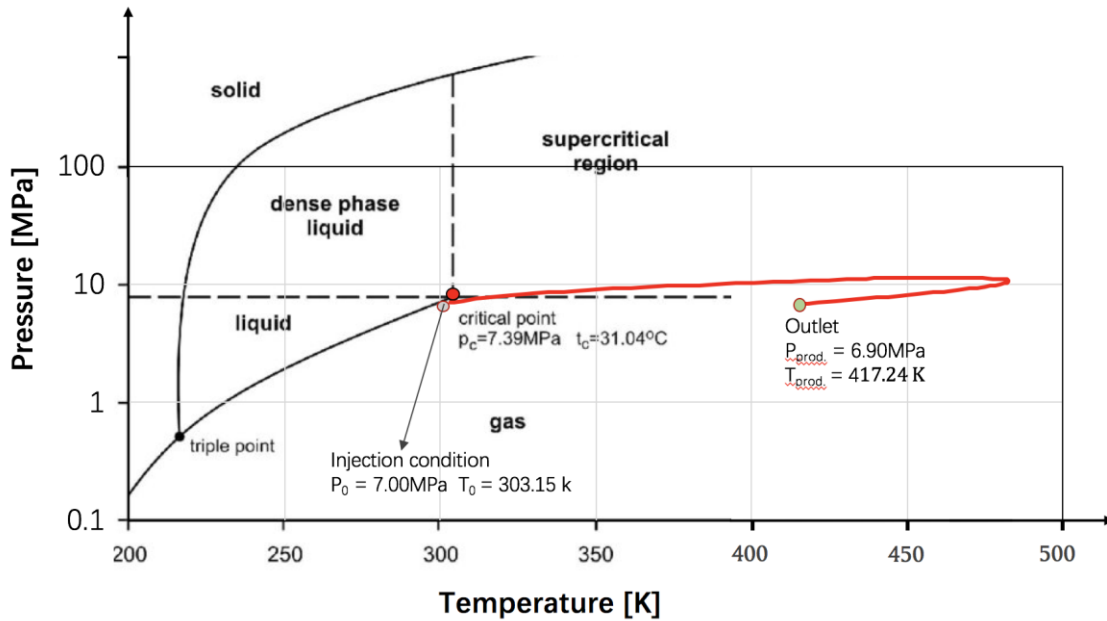


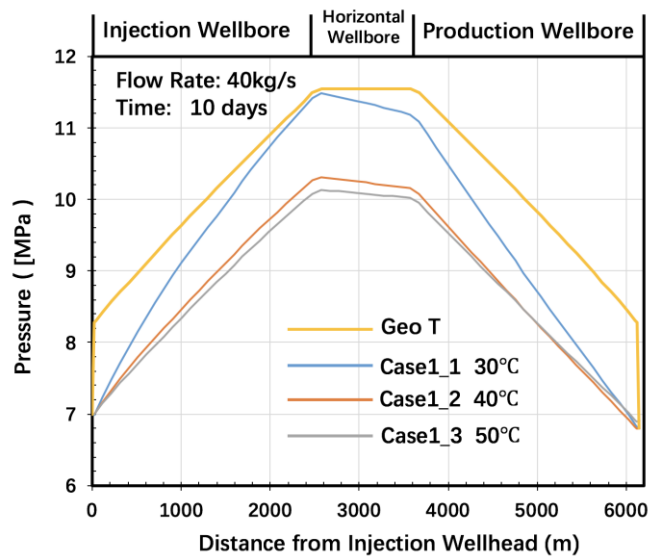
Figure 23. Thermal cycle from inlet to outlet in the CO₂ phase diagram under 80kg/s mass flow rate (Case3_1).

From Figure 23, we can observe the temperature profile along injection wellbore almost be around the boundary of two areas (supercritical and subcritical), and it's unclear that how to judge the boundary between subcritical phase and supercritical phase. Plus, the density of supercritical CO₂ is close to liquid and the density of subcritical CO₂ is close to gas. Therefore, there must be a huge density change occurs at the point that subcritical phase become to supercritical phase completely (like the red cycles marked in Figure 22. which indicate phase transition).

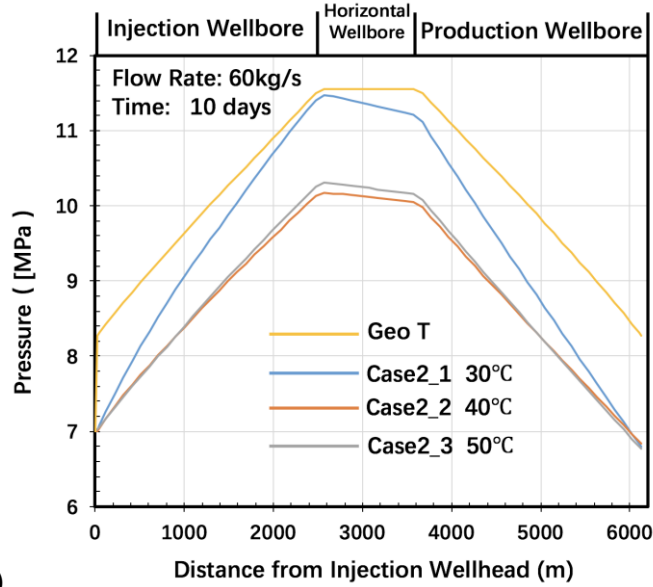
Also, it is clear that density profile of CaseX_1 are always higher than CaseX_2 and CaseX_3 from 0 m nearly until 5800 m (Finally, the CaseX_1 reach the lowest density at outlet among other cases), which means the density difference (ΔD_1) of CaseX_1 is much high than ΔD_2 of CaseX_2 and ΔD_3 of CaseX_3 (see Figure22. (c) as an example). In the other words, CaseX_1 has the biggest density difference in the production wellbore, which means CaseX_1 has the biggest natural driving force. Therefore, the mass flow rate of CaseX_1 along production wellbore is the highest among all cases. It is considered that the CO₂ ascending of CaseX_1 along production wellbore will spend shorter time than other cases. That's mean heat loss time of

CaseX_1 in production wellbore is less than other cases. That's the reason why temperature decreasing rate of CaseX_1 is less than CaseX_2 and CaseX_3.

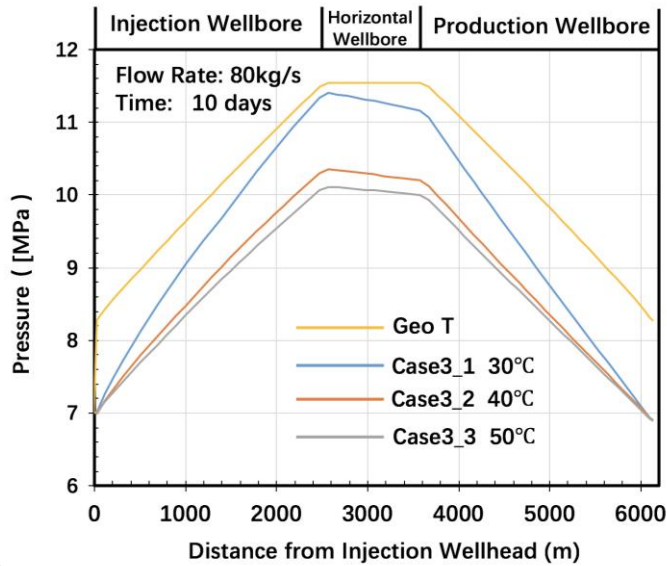
As to pressure profile, although the pressure at inlet and outlet are set to constant, pressure values from 0 m to 6100 m of CaseX_1 are always higher than other two cases. In CaseX_2 and CaseX_3, CO₂ is injected in subcritical phase, and the property of them is close to gas. However, in CaseX_1 CO₂ at inlet is still in liquid phase, compared to gas phase of CaseX_2 and CaseX_3, CaseX_1 can keep higher pressure profile throughout 6100 m wellbore until decreasing to the same pressure value at outlet with other cases. Combine density profile (Figure 22) and pressure profile (Figure 24), they show high density is related to high pressure because density of CaseX_1 keep bigger than CaseX_2 and CaseX_3. Therefore, pressure profile of CaseX_1 shows the similar trend that higher than other cases throughout 6100 m length and converge to almost equal value at outlet.



(a)



(b)



(c)

Figure 24. Simulation results of the effect of different CO₂ injection temperature on pressure change in closed loop under different mass flow rate.

Mass flow rate: (1) 40kg/s; (2)60kg/s; (3)80kg/s. **Injection temperature:** (1) 30°C; (2) 40°C; (3) 50°C.

In order to show there actually CO₂ in production wellbore has different velocity when it flows up, we show the velocity of 9 subcases along production wellbore in Figure 25. In Figure 25(a) and Figure 25(c), it is obvious that velocity of Case1_1 and Case3_1 are higher than other subcases, and although velocity of Case2_2 is higher than Case2_1 temporarily at the beginning in Figure25(b), Case2_1 exceed Case2_2 at 4400 m and widen the gap persistently. Therefore, short ascending time in wellbore due to high velocity can be explained as one of the important reasons, because it brings

the amount of heat loss down when CO₂ flow up to outlet.

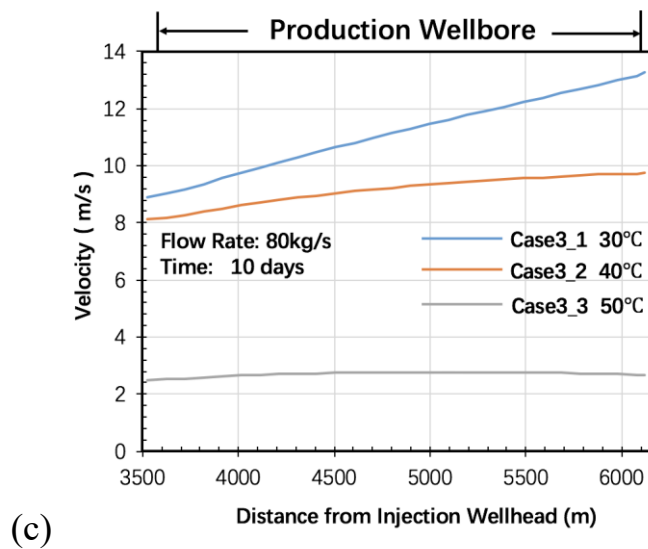
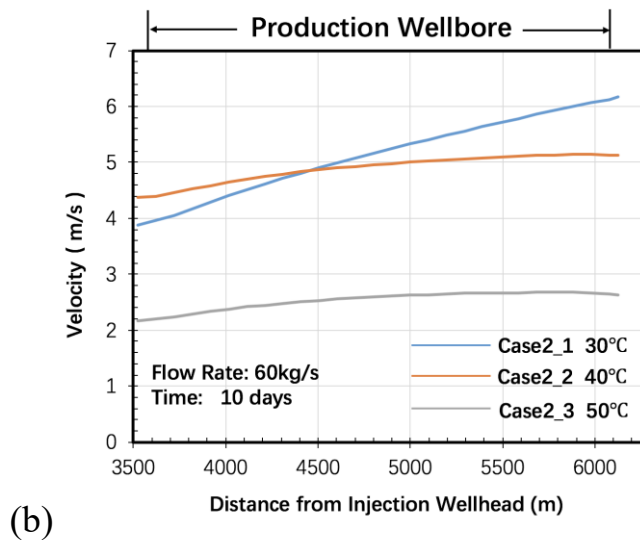
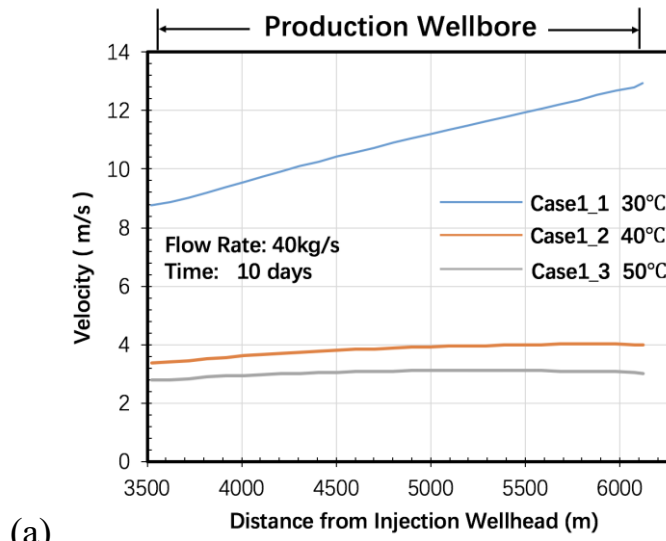
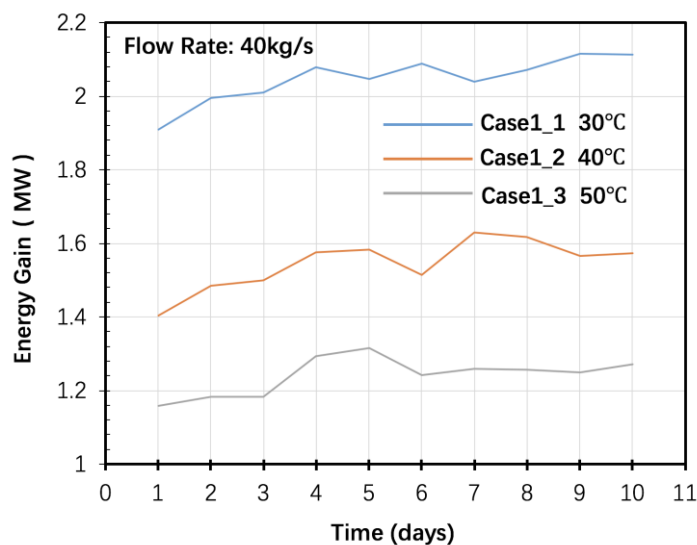


Figure 25. Simulation results of the effect of different CO₂ injection temperature on pressure change in closed loop under different mass flow rate.

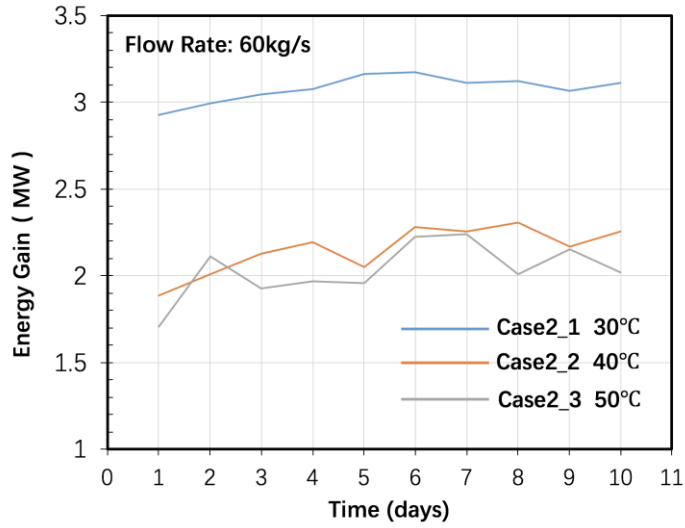
4.3 Energy Gain

We have used a detailed coupled pipe-reservoir model T2Well to investigate the effects of mass flow rate and injection temperature on the energy gain of CO₂ flowing in a U-shaped well through a geothermal reservoir. Whether the condition of CO₂ at inlet is critical (super- or sub-) phase or not is a primary control on energy gain by the working fluid, with natural convection strongly favoring heat transfer to fluid in the pipe. Because of compressibility, the energy gain by flowing CO₂ in the wellbore is a complicated function of initial temperature, pressure and mass flow rate in our simulation.

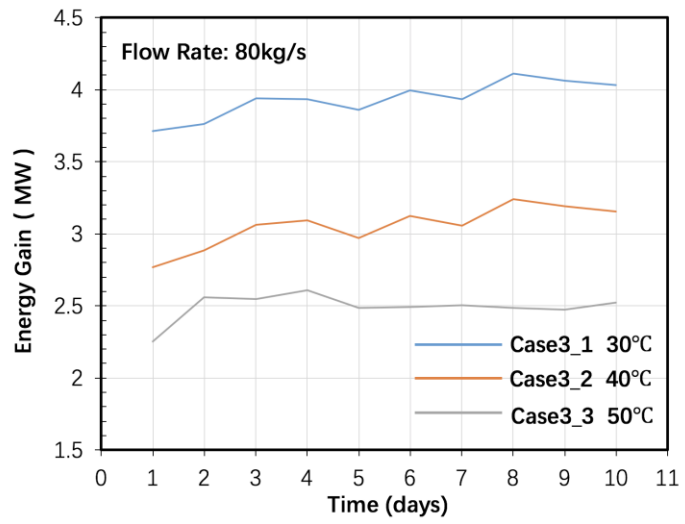
From Figure 26, We can find the flow rate of 80 kg/s (Case 3) is the most that can achieve energy at outlet, and injection temperature of 30°C is the most effective among Case3. Here, we can conclude that high mass flow rate will produce more energy and low injection temperature will gain more heat from reservoir within a certain range. However, variables considered included pipe diameter, well depth, horizontal well length, temperature gradients, flow rates, pressures and so on. We should fix several parameters and test the characteristic of rest important parameters, thus we can optimize a range of parameters to gain the most energy under fixed condition.



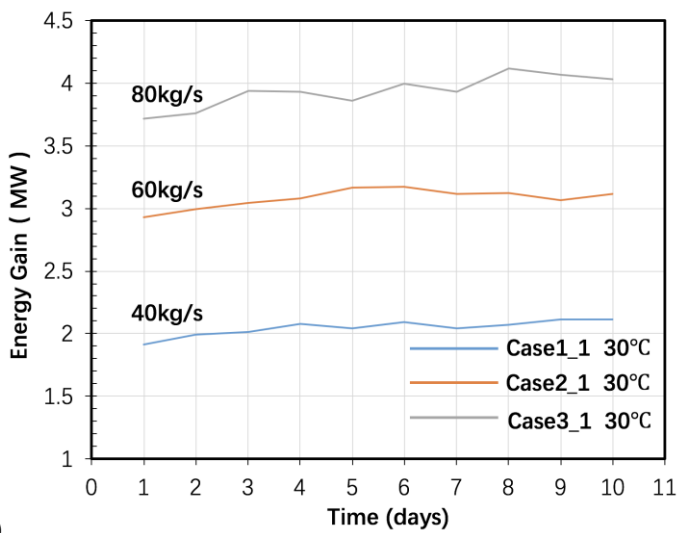
(a)



(b)



(c)



(d)

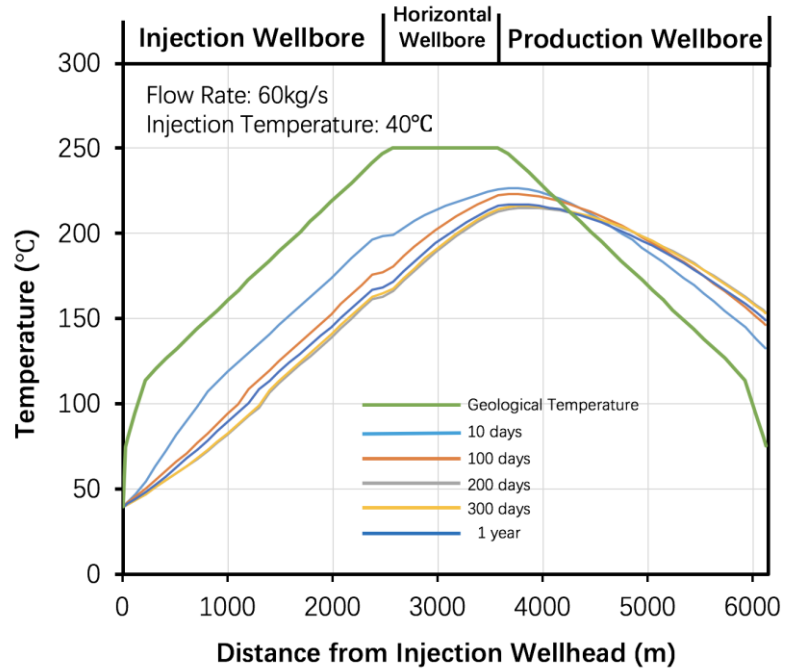
Figure 26. Simulation results of energy gain for various CO₂ flow rates and injection temperature under the same injection pressure.

4.4 Sustainability

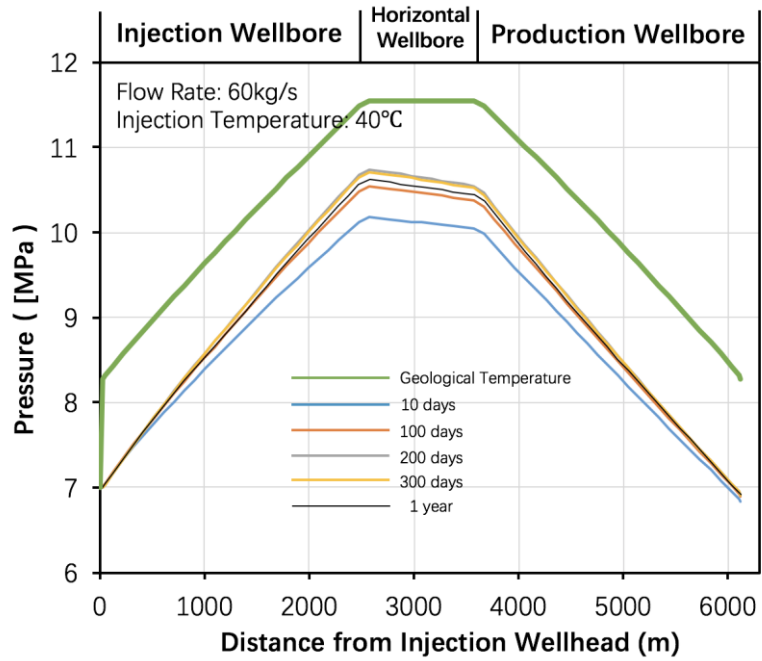
we have known that closed loop geothermal system can provide nearly steady energy output during 10 days. However, considering the indicators that affect sustainability of power generation and plant operation, which usually will be based upon environmental and societal impacts, greenhouse gas emissions, resource depletion, availability of the energy sources, and the value that they add to the economy. Here, we focus on resource depletion and the value can be contributed to economy because this is a closed loop system rather than open system which has the concerns about environmental problems (issues like seismic, toxic pollutants and GHG emissions).

First, for resource depletion we choose “energy output” as key indicator, see profile of temperature, pressure, density as significant indicators to investigate whether energy output can keep or not which is no less than average value of energy gain during initial 10 days.

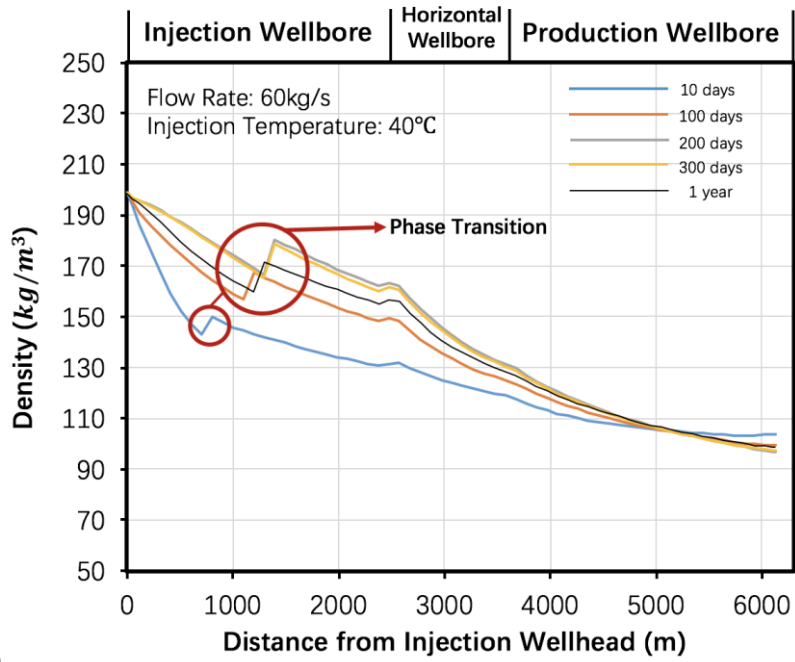
As seen in Figure 27a, compared to temperature profile of 10th days, all the temperature value until the point around the bottom of production wellbore in later operation has low value than 10th days’. But finally the temperature at outlet (6100 m) of longer time simulation all become bigger than 10th day’s result. Then as shown in Figure 27b, pressure values of long-time simulation are nearly almost bigger than 10th days’ from 0 m to 6100 m until become same at outlet since pressure at outlet has been set to the fixed. Next, as to density term, density values of long-time simulation are always bigger than 10th days’ values before about 5000 m and forms larger density difference between inlet and outlet than 10th days’ results. By the way, there is something interesting occurs that when the phase transition takes places at deeper and deeper evaluation along injection wellbore, the density values are higher according to Figure 27c. At last, in Case2_2 we find the value (about 2.58WM) of energy gain in geothermal operation after 1 year is higher than the value (2.25MW) of energy gain after 10 days, which indicates there is no resource depletion occurred in the closed loop system within a year.



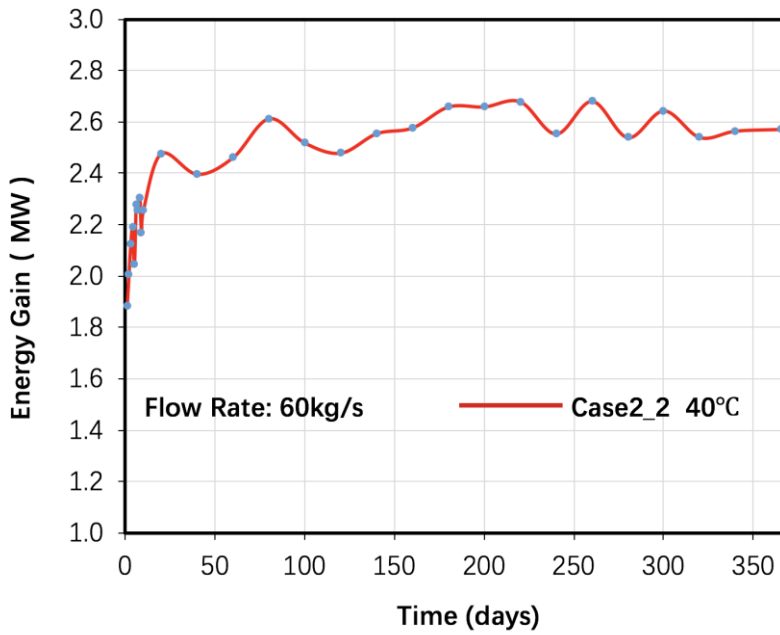
(a)



(b)



(c)



(d)

Figure 27. Four significant parameters simulated for 1 year to demonstrate the sustainability of steady geothermal energy output. (All results come from the Case2_2)

- (a) Temperature change profile within 1 year; (b) Pressure change profile within 1 year;
(c) Density change profile within 1 year; (d) Energy change profile within 1 year.

4.5 Cost and Profit

In this study, we know low injection temperature (especially in liquid phase) will extract more energy within certain range and high mass flow rate can lead to more energy gain under **practicable** range. However, even though we master this kind of applicable law, it can't be commercialized as soon as possible if the balance between cost and profit is not calculated (estimated). Therefore, here we need to do a cost estimation and give a specific range of profit that the closed loop geothermal system gives.

In general, the CO₂-based system is found to be very sensitive to both assumptions in the pricing model (particularly well costs), and to process operational parameters. We use an Economic/Costing Methodology provided by The Queensland Geothermal Energy Centre of Excellence. Economic analysis of the project is conducted based on standard process engineering cost methodologies. Where appropriate, upper and lower bounds for cost estimates are used to provide insight into costing results. Upper bounds represent a range where all uncertainties in cost estimation are taken as the unfavorable. Lower bounds represent the favorable end of cost uncertainties. Here, the Total Capital cost includes three main factors ---- "Heat Exchanger Costs, Turbine Costs and Well Costs".

4.5.1 Heat Exchanger Costs

The base costs of the heat exchangers are estimated from standard costing methods (Turton, Bailie et al. c2003). The approach is reproduced here for clarity. Costing is based on air-cooled heat exchangers and in some cases water cooling will be available. In this cases, the cost of cooling systems will be significantly reduced. The cost of heat exchangers is estimated from:

$$C_{BM,HX} = (B_1 + B_2 F_M F_P) C_P^0 \quad (45)$$

Where $C_{BM,HX}$ is the bare module cost, B_1 , and B_2 are constants for an equipment type, F_M is the material factor, F_P is the pressure factor, and C_P^0 is the cost for the same equipment made from carbon steel operating at ambient pressure. The constants used in this cost analysis (Stainless steel equipment) are given in Table 9.

Table 9: Constants for heat exchanger costs

Exchanger Type	B_1	B_2	F_M
Air-Cooled	0.96	1.21	2.9

In this study, we adopt shell and tube heat exchanger to exchange heat between hot CO₂ and clean process fluid which is shown as follows (Figure 28):

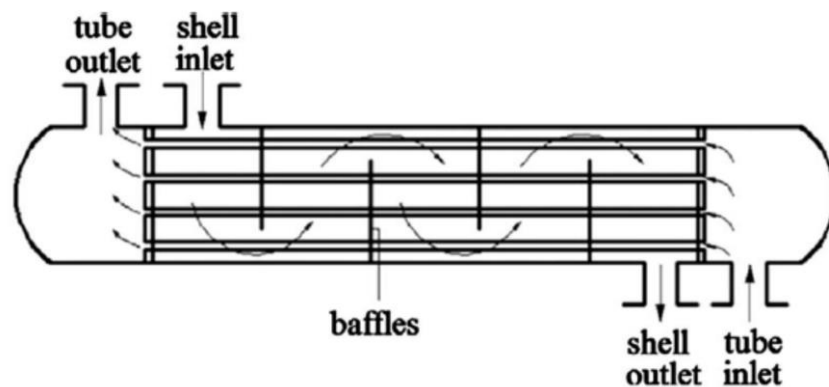


Figure 28. Shell and tube heat exchanger

And the parameters of heat exchanger are written in Table 10:

Table 10. Typical values of the variables for the shell and tube heat exchangers in ORC application.

Variable	Lower boundary	Upper boundary
Shell diameter (D)	0.3 m	2 m
Tube outside diameter (d)	5 mm	50 mm
Relative tube pitch (p/d)	1.2	2.5
Ratio length/shell diameter (L/D)	6	10
Ratio of tube diameter to shell diameter	0.001	0.1

The base cost for carbon steel equipment is given by:

$$C_p^0 = 10^{(K_1 + K_2 \log A + K_3 \log [A]^2)} \quad (46)$$

where K_1 , K_2 and K_3 are constants for the heat exchanger type, and A is the area of the heat exchanger. The constants are given in Table 11.

Table 11: Constants for heat exchanger base costs

Exchanger Type	K_1	K_2	K_3
Air-Cooled	4.0336	0.2341	0.0497

Area for these estimations is limited to 10,000 m² for the air-cooled heat exchanger. Above these sizes of equipment, costs will be linearly extrapolated from an equipment size of 10,000 m². Pressure factors are given by the equation:

$$F_p = 10^{(C_1 + C_2 \log P + C_3 \log [P]^2)} \quad (47)$$

Where C_1 , C_2 and C_3 are constants for the heat exchanger type, and P is the design pressure (bar) of the equipment. The values of these constants are given in Table 12.

Table 12: Constants for heat exchanger pressure factors

Exchanger Type	C ₁	C ₂	C ₃
Air-Cooled	-0.1250	0.15361	-0.02861

The range of pressure factor estimation is specified as limited to below 1000 MPa for air-cooled heat exchangers. As some design pressures for the CO₂ thermosiphon may be slightly above this range, a small extrapolation of these pressure factors is used. The extrapolation is derived from the fit of a power law to the higher-pressure region (i.e. 500~1000 MPa) of the pressure-factor calculation, which is then extrapolated. The resulting equation for the extrapolation is:

$$F_p = 0.9396P^{0.04759} \quad (48)$$

Therefore, we calculate the heat exchanger costs according to the formula prompted above. First, because injection pressure by pump is 0.7 bar:

$$F_p = 0.9396P^{0.04759} = 0.9396 \times 0.7^{0.04759} = 0.9396 \times 0.9832 = 0.9238$$

Second,

$$\begin{aligned} C_p^0 &= 10^{(K_1 + K_2 \log A + K_3 \log [A]^2)} = 10^{(4.0336 + 0.2341 \log 10000 + 0.0497 \log [10000]^2)} \\ &= 10^{(4.0336 + 0.9364 + 0.3976)} = 233130.986 \end{aligned}$$

Then,

$$\begin{aligned} C_{BM,HX} &= (B_1 + B_2 F_M F_p) C_p^0 = (0.96 + 1.21 \times 2.9 \times 0.9238) \times 233130.986 \\ &= 4.2016 \times 233130.986 = 979523.151 \text{ USD} \end{aligned}$$

4.5.2 Turbine Costs

A method of estimating the costs of CO₂ turbines was formulated in an earlier work (Atrens, Gurgenci et al. 2009). That method accounted for the higher density of CO₂ under the thermodynamic conditions within the turbine, leading to lower equipment size. To apply the results of that method directly in an easy-to-calculate manner, the following equation for the turbine cost was formulated:

$$C_{BM,T} = \alpha W_T F_S = \alpha W_T^\beta \rho_{out}^\gamma \quad (49)$$

where C is the bare module cost of the turbine, W_T is the turbine work output, α and β and γ are constants, and F_S is the size factor, and is dependent on turbine outlet density (ρ). This equation was fitted to the costs of steam turbines and CO₂ turbines estimated in the previous work (Atrens, Gurgenci et al. 2009). The quality of the fit is presented in Figure 29.

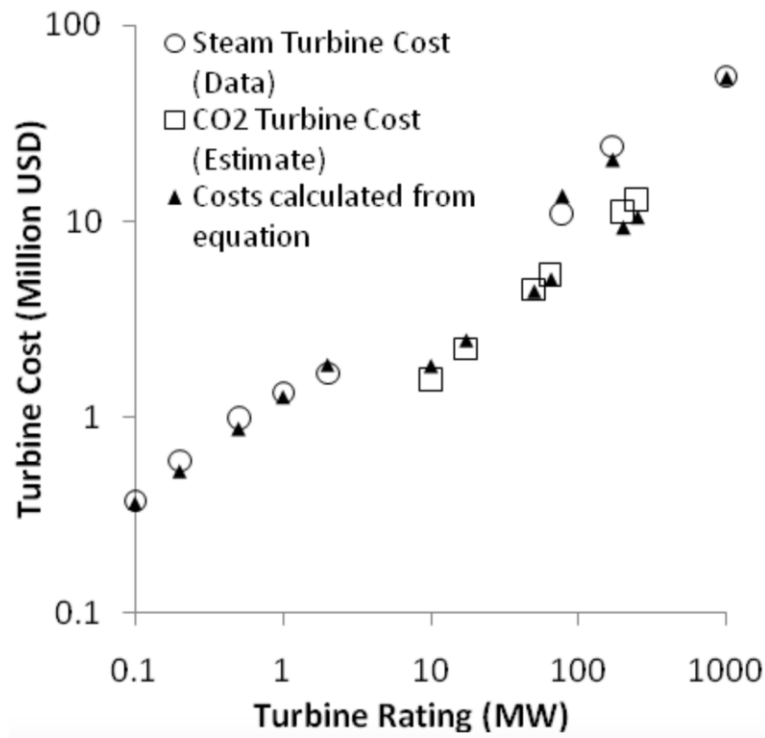


Figure 29. Turbine costs estimated from equation 49

The minimization of least squares to provide this fit of data resulted in constants for equation 49 as given in Table 13.

Table 13: Turbine cost equation constants

α	β	γ
1.066	0.5439	-0.1472

This provides an estimate for the cost of CO₂ turbines that fits reasonably with the understanding of the equipment and the fluid conditions involved.

However, in this study, the turbine work output is estimated by relatively new model of geothermal turbine and based on binary plants which are closed cycles that converts heat from the geothermal fluid into electricity by transferring the heat to an organic working fluid, and then produces vapor to generate electricity. According to Department of Engineering Science, University of Auckland, the title named “Efficiency of Geothermal Power Plants: A Worldwide Review”, it is calculated that turbine efficiency is 54%~62%. Therefore, here we use Case3_1 which has the highest output energy as an example to demonstrate how to operate.

$$C_{BM,T} = \alpha W_T F_S = \alpha W_T^\beta \rho_{out}^\gamma = 1.066 \times (4000000 \times 54\%)^{0.5439} \times 100^{-0.1472}$$

$$= 1.066 \times 2788.1067 \times 0.1837 \times 10^3 = 545.9788 \times 10^3 \text{ USD}$$

4.5.3 Well Costs

GreenFire Energy's Well Retrofit Solution generates power from existing hydrothermal wells that are idle or underproductive. Globally, over 20% of geothermal wells are underproductive either from inception or due to degradation over time. Well Retrofits comprise a flexible system of components and processes that can be employed in a variety of configurations to optimize geothermal power production from a wide spectrum of well conditions without the risk and cost of drilling. GreenFire Energy Inc.'s innovative ECO2G™ geothermal well retrofit technology will enable geothermal project owners to generate power from idle or marginal wells at low risk and attractive cost per MWh. Success in geothermal well retrofits will eventually enable GreenFire to develop large-scale ECO2G projects in more locations.

ECO2G technology harnesses recent advances in deep and directional drilling technologies from the oil and gas industry to access geothermal resources that cannot be developed with existing geothermal technology. The demonstration project involves inserting a co-axial closed-loop tube into an existing geothermal well that lacks sufficient pressure and permeability to generate power. Various refrigerants including supercritical carbon dioxide (SCCO2) will then be circulated to transfer heat to the surface and generate power from a small turbo expander.

The cost of well is calculated with

$$C_{\text{well}} = Ke^{bz}(1 - \xi) + \left(\frac{D}{D_0}\right)^2 \xi Ke^{bz} \quad (16)$$

where C_{well} is the cost of the well, z is the well depth, D is the well diameter, D_0 is a standard diameter used as a baseline, ξ is the fraction of time spent drilling out of total time, and K and b are constants from the relationship between cost and depth.

Table 14: Well cost equation constants

K	b	ζ
0.554	0.000613	0.25

ζ is of course variable, and depends on the characteristics of the rock, amount of difficulties, etc. For this analysis, it is kept at a base value of 25%, as this is similar to estimates for geothermal wells (Polsky, Mansure et al. 2009).

Therefore, we can see it take almost \$15~17 million USD to build the 6100m wellbore from Figure 30.

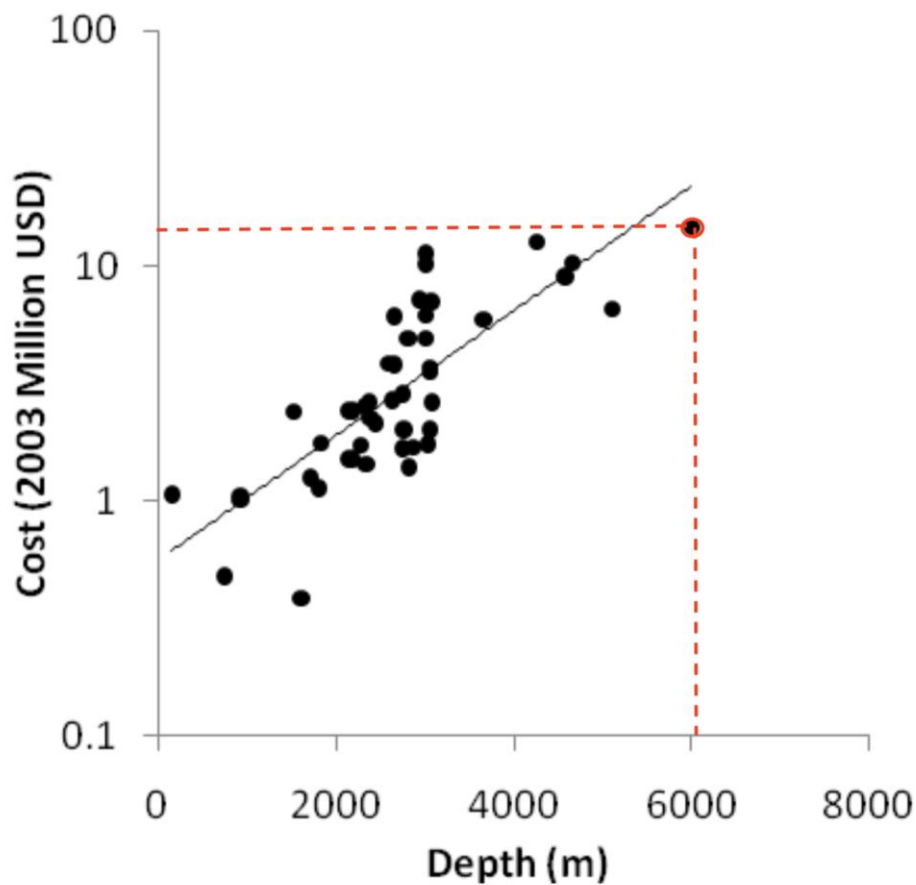


Figure 30. Well cost (2003 \$M) versus depth (m), with fit line

4.5.4 Total Capital cost

This work provides a starting point for optimization of CO₂-based ECO2G for economic performance. The total capital cost of the power plant is estimated from the equation:

$$C_{TOT} = \omega(C_{BM,HX} + \lambda C_{BM,T}) + \sum_i^n C_{well,i} \quad (44)$$

Where C_{CON} is the total capital cost, ω is a constant to take into account the cost increase of building a green-fields facility, λ is a constant to scale up the turbine cost with additional piping, control, freight, labor, and other overheads, and n is the number of wells. The values of the two constants are given in Table 8. Well costs are increased by a factor of 1.093 to account for inflation from 2003 to 2006 (due to lack of a geothermal drilling cost index for 2006).

Table 15: Constants used in overall cost estimation

ω	λ
1.8	2.4

In this study, the most efficient case is Case3_1 which almost has the 4MW energy output, and converts into 1MWe according to 25% general thermoelectric conversion rate. The unit price of electricity from geothermal power generation is \$0.3/kW (plant scale under 15MW) or \$0.2/kW (plant scale beyond 15MW) with all equipment renewal type replacement under the FIT System.

However, here we haven't sufficient data (eg. new model equipment models, local tax rate and the numbers of wellbore) so that accurate initial cost and operational cost can't be calculated in this study. Furthermore, more specific and comprehensive cost for a long time need to be included to calculate in next step.

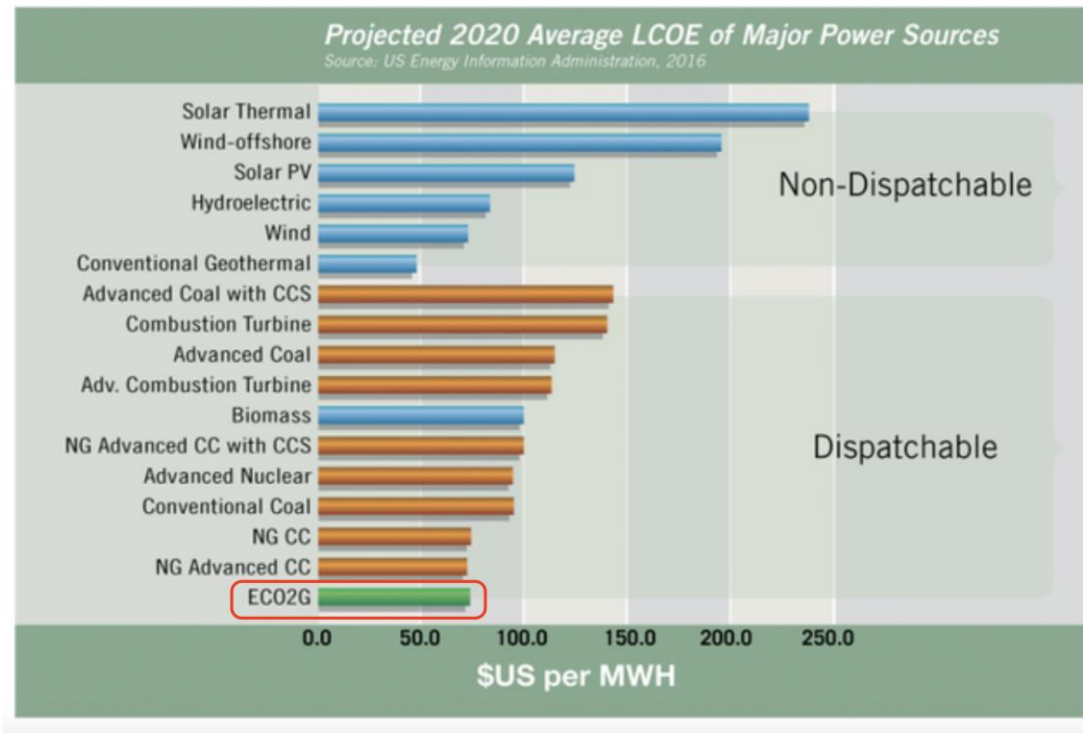


Figure 31. Projected 2020 Average Levelized Cost of Electricity of Major Power Sources from US Energy Information Administration, 2016

From above calculation according to The University of Queensland, The Queensland Geothermal Energy Centre of Excellence, we find it is perhaps not in accordance with actual ECO2G situation. As a result, we choose to adopt projected 2020 average levelized cost of electricity of major power sources from US Energy Information Administration as the basis of calculation.

As shown in Figure 31, we know it will take \$0.065~0.075 per KWH. Compared with conventional unit price of electricity (\$0.2~0.3 per KW), the unit price of electricity by ECO2G method is much lower, which can show economic advantages that ECO2G has.

We need to consider more possible cost that will be necessary for long-time operation (eg. Operating years, maintenance, equipment renewal fee, tax, environmental improvement costs and so on), which are full of uncertainty. Therefore, in order to give more appropriate and accurate cost estimation, we must consider more critical and significant factors to complete a long-time calculation.

Chapter 5: Conclusion

We have used a detailed coupled pipe-reservoir model to investigate the effects of various parameters on the energy gain of CO₂ flowing and the sustainability of steady energy output in a U-shaped well through a geothermal reservoir. Although we know there are many factors strongly control the performance of geothermal system, it shows injection temperature and mass flow rate are primary control on energy gain by the working fluid in this study, with CO₂'s phase transition strongly favoring heat gain due to energy conversion (pressure energy to thermal energy) and high velocity in the pipe. Because of phase transition, the energy gain by flowing CO₂ in the pipe is becoming more efficient, but how to control phase transition for best energy gain is tested in this study. We found there are always phase transition occurs in our cases, especially the cases that CO₂ were injected into wellbore in liquid state. Rather than injection condition supercritical/subcritical whose state is close to gas, injection in liquid phase (under critical point) can cause greater density difference between inlet and outlet as a result of stronger driving force which is explicitly expressed as high velocity that can decrease heat loss time in production wellbore, and in spite of pressure values in inlet and outlet have been fixed for all cases, it can keep higher pressure profile from inlet to outlet, which is considered energy conversion exists, pressure energy converts into thermal energy, so that liquid injection cases have more energy gain than other cases.

As a conclusion, low injection temperature (under critical point with injection pressure) and high mass flow rate can bring more benefit to energy gain. Especially, liquid injection condition is better for heat extraction. Meanwhile, we tried to investigate whether the energy output in such a closed loop geothermal system steady or not by simulating 1-year system operation, the results are even there actually slight fluctuation for the values of the energy output occur over time, but it is nearly approach to the steady curve. Furthermore, we need to do more investigation in order to understand why fluctuations occur.

Finally, we tried to do some calculation/estimation for cost and profit, but specific values for cost and profit didn't get from our estimation due to lack of equipment data and other empirical parameters. Therefore, we will do further calculation in future work.

REFERENCES

- [1] Karsten Pruess, Curt Oldenburg, Geoge Moridis, TOUGH2 USER'S GUIDE, VERSION2.0, Lawrence Berkeley National Laboratory Report, LBNL-43134, November 1999.
- [2] Pan, L., 2003. Wingridder-an interactive grid generator for TOUGH2. Lawrence Berkeley National Laboratory. Pan, L., and C.M. Oldenburg. "T2Well—An integrated wellbore–reservoir simulator." *Computers & Geosciences* 65 (2014), 46-55.
- [3] Azadeh Riahi, Piotr Moncarz, Walter Kolbe, Branko Damjanac, Innovative Closed-Loop Geothermal Well Designs Using Water and Super Critical Carbon Dioxide as Working Fluids, 2017.
- [4] Oldenburg, C.M., and L. Pan, Porous Media Compressed-Air Energy Storage (PM-CAES): Theory and Simulation of the Coupled Wellbore–Reservoir System, *Transport in Porous Media*, 97(2) 201-221, 2013.
- [5] Oldenburg Curtis, Pan Lehua, Muir Mark et al. Numerical Simulation of Critical Factors Controlling Heat Extraction from Geothermal Systems Using a Closed-Loop Heat Exchange Method. Stanford University, Stanford, California, February 22-24, 2016.
- [6] Aleks D. Atrens, Hal Gurgenci and Victor Rudolph, Economic Analysis of CO₂ Thermosiphon, *Proceedings World Geothermal Congress* 2010.
- [7] Lehua Pan, Curtis M. Oldenburg, Yu-Shu Wu¹ and Karsten Pruess, T2Well/ECO2N Version 1.0: Multiphase and Non-Isothermal Model for Coupled Wellbore-Reservoir Flow of Carbon Dioxide and Variable Salinity Water, 2011.
- [8] GEORGE J.MORIDIS and KARSTEN PRUESS, T2SOLV: AN ENHANCED PACKAGE OF SOLVERS FOR THE TOUGH2 FAMILY OF RESERVOIR SIMULATION CODES,1998.

- [9] George J. Moridis, USER'S MANUAL OF THE MESHMAKER v1.5 CODE: ^[1]_{SEP}A MESH GENERATOR FOR DOMAIN DISCRETIZATION IN SIMULATIONS OF THE TOUGH+ AND TOUGH2 FAMILIES OF CODES, 2016.
- [10] Curtis M. Oldenburg, Lehua Pan, Mark P. Muir, Alan D. Eastman, Brian S. Higgins, Numerical Simulation of Critical Factors Controlling Heat Extraction from Geothermal Systems Using a Closed-Loop Heat Exchange Method, 2016.
- [11] Finsterle Stefan, Yingqi Zhang, Lehua Pan, Patrick Dobson, Ken Oglesby (2013). Microhole arrays for improved heat mining from enhanced geothermal systems. *Geothermics* 47 (2013) 104–115.
- [12] Litang Hu, Lehua Pan, Keni Zhang (2012), Modeling brine leakage to shallow aquifer through an open wellbore using T2WELL/ECO2N. *International Journal of Greenhouse Gas Control* 9 (2012) 393–401. ^[1]_{SEP}
- [13] Yingqi Zhang, Lehua Pan, Karsten Pruess, Stefan Finsterle (2011) A time-convolution approach for modeling heat exchange between a wellbore and surrounding formation. *Geothermics*. doi:10.1016/j. geothermics. 2011.08.003. ^[1]_{SEP}
- [14] Lehua Pan, Curtis M. Oldenburg (2012), T2Well—An Integrated Wellbore-Reservoir Simulator. PROCEEDINGS, TOUGH Symposium 2012 Lawrence Berkeley National Laboratory, Berkeley, California, September 17-19, 2012.
- [15] Pan, L. Curtis M. Oldenburg, Yu-Shu Wu, Karsten Pruess. 2009. Wellbore flow model for carbon dioxide and brine. *Energy Procedia* 1(1):71-78.
- [16] Pan, L., 2008, User's Information for WinGridder V3.0. LBNL-273E.
- [17] Pan, L., 2003. WinGridder - An interactive Grid Generator for TOUGH2. Proceedings, TOUGH Symposium 2003. Berkeley, CA: pp. 6 LBNL-52422.
- [18] Barry M. Freifeld, Lehua Pan, Christine Doughty, Steve Zakem, Kate Hart, Steve Hostler.,2016. Demonstration of Geothermal Energy Production

Using Carbon Dioxide as a Working Fluid at the SECARB Cranfield Site, Cranfield, Mississippi.

[19] Karsten Pruess., 2013. ECO2M: A TOUGH2 Fluid Property Module for Mixtures of Water, NaCl, and CO₂, Including Super- and Sub-Critical Conditions, and Phase Change Between Liquid and Gaseous CO₂.

[20] Coso, California., 2018. GreenFire Energy Demonstration Project.

[21] Aleks D. Atrens, Hal Gurgenci and Victor Rudolph.,2010. Economic Analysis of CO₂ Thermosiphon.

[22] Karsten Pruess, Curt Oldenburg and George Moridis.,1999. TOUGH2 USER'S GUIDE, VERSION 2.0, LBNL-43134.

[23] Finsterle S., C. Doughty, M.B. Kowalsky, G.J. Moridis, L. Pan, T. Xu, Y. Zhang, and K. Pruess, 2008, Advanced Vadose Zone Simulation Using TOUGH. Vadose Zone Journal 7:601-609. [\[1\]](#) [\[SEP\]](#)

[24] Pan, L., and G. S. Bodvarsson, 2002. Modeling transport in fractured porous media with random-walk particle method: The transient activity range and the particle transfer probability, Water Resource Research, 38(6):1029-1035. [\[1\]](#) [\[SEP\]](#)

[25] L Pan, B Freifeld, C Doughty, S Zakem, M Sheu, B Cutright, T Terrall (2015). Fully coupled wellbore-reservoir modeling of geothermal heat extraction using CO₂ as the working fluid. Geothermics 53, 100-113. doi:10.1016/j. geothermics.2014.05.005. [\[1\]](#) [\[SEP\]](#)

謝辞

まず、本研究を行うにあたり、ご指導ご鞭撻してくださいました指導教員の愛知正温講師に心より深く感謝いたします。研究の面で行き詰まったところがあると、いつも親身になって話を聞いていただき、的確な助言をしていただきました。また、日頃は学生のことを信じて暖かく見守って下さり、研究に主体的に向き合える環境を提供していただきました。この場を借りて、心より感謝申し上げます。

そして、熱心なご指導をしてくださいましたどう研究室の先輩 志賀正茂さん、秋田谷健人さん、森垣勇人さん、森川慎也さん、Michel Yu Chavez Okadaさんに心より厚く御礼申し上げます。研究生生活のサポートや研究室の日常イベントなど場面でも、多方面からの学びを与えていただき、大変感化されました。この場を借りて、感謝の意を述べさせていただきます。

環境システム学専攻にいるこの三年半間、愛知研究室の後輩である楊舒翔君、趙麗園さん、張開元君、桑杉さん、川崎敬君、角野愛美さん、Feilula Haishaerさんに、数ヶ月から数年までにわたり大変お世話になりました。心より感謝申し上げます。また、愛知研究室特任研究員である Joshi Ajit さんに、長い間で自分の研究を指導して頂くことに厚く御礼申し上げます。

そして、2017年10月入学の同期である、多部田研の馮子卿君、大島研の劉源君、井原研の張典君には2.5年間で迷惑をかけることも多くありましたが、私にとってその存在はとても大きく、この感謝の気持ちは言葉では言い表せません。

部田研の卒業生である岩場公利様、内田恵様、須田紗耶加様にも、2020年4月卒業の同期である三木皓貴、萩野誠一郎在学中は多大なるご厚意を賜りました。心より感謝いたします。また、多部田研究室の大先輩である久松力人さん、鈴木翔太さん、張宇さんには日頃の学生生活で大変お世話になりました。

最後に、20年以上にわたって支えてくれた両親や親友達に、心より深く感謝いたします。

